Secrecy-Energy Efficient Hybrid Beamforming for Satellite-Terrestrial Integrated Networks

Zhi Lin, Min Lin, *Member, IEEE*, Benoit Champagne, *Senior Member, IEEE*, Wei-Ping Zhu, *Senior Member, IEEE*, and Naofal Al-Dhahir, *Fellow, IEEE*

***Abstract*—In this paper, we investigate secrecy-energy efficient hybrid beamforming (BF) schemes for a satellite-terrestrial integrated network, wherein a multibeam satellite system shares the millimeter wave spectrum with a cellular system. Under the assumption of imperfect angles of departure for the wiretap channels, the hybrid beamformer at the base station and digital beamformers at the satellite are jointly designed to maximize the achievable secrecy-energy efficiency, while satisfying signal-to-interference-plus-noise ratio constraints of both the earth stations (ESs) and cellular users. Since the formulated optimization problem is nonconvex and mathematically intractable, we propose two robust BF schemes to obtain approximate solutions with low complexity. Specifically, for the case of a single ES, we integrate the Charnes-Cooper approach with an iterative search algorithm to convert the original nonconvex problem into a solvable one and obtain the BF weight vectors. In the case of multiple ESs, by exploiting the sequential convex approximation method, we convert the original problem into a linear one with multiple matrix inequalities and second-order cone constraints, for which we obtain a solution with satisfactory performance. The effectiveness and superiority of the proposed robust BF design schemes are validated via simulations using realistic satellite and terrestrial downlink channel models.**

***Index Terms*—Hybrid analog-digital beamforming, robust design, satellite-terrestrial integrated network, secrecy-energy efficiency.**

Manuscript received January 12, 2021; revised April 24, 2021; accepted June 7, 2021. Date of publication June 14, 2021; date of current version September 16, 2021. This work was supported in part by the National Natural Science Foundation of China under Grant 61901490, in part by the Key International Cooperation Research Project under Grant 61720106003, in part by the Shanghai Aerospace Science and Technology Innovation Foundation under Grant SAST2019-095, and in part by the NUPTSF under Grant NY220111. The associate editor coordinating the review of this article and approving it for publication was F. J. Lopez-Martinez. *(Corresponding author: Min Lin.)*

Zhi Lin is with the Institute of Electronic Countermeasure, National University of Defense Technology, Hefei 230037, China (e-mail: linzhi945@163.com).

Min Lin is with the School of Communication and Information Engineering, Nanjing University of Posts and Telecommunications, Nanjing 210003, China (e-mail: linmin@njupt.edu.cn).

Benoit Champagne is with the Department of Electrical and Computer Engineering, McGill University, Montreal, QC H3A 0G4, Canada (e-mail: benoit.champagne@mcgill.ca).

Wei-Ping Zhu is with the Department of Electrical and Computer Engineering, Concordia University, Montreal, QC H3G 1M8, Canada, and also with the School of Communication and Information Engineering, Nanjing University of Posts and Telecommunications, Nanjing 210003, China (e-mail: weiping@ece.concordia.ca).

Naofal Al-Dhahir is with Department of Electrical and Computer Engineering, The University of Texas at Dallas, Richardson, TX 75080 USA (e-mail: aldhahir@utdallas.edu).

Color versions of one or more figures in this article are available at https://doi.org/10.1109/TCOMM.2021.3088898.

Digital Object Identifier 10.1109/TCOMM.2021.3088898

I. Introduction

IN RECENT years, terrestrial cellular networks have experienced explosive growth in wireless data traffic. With the proliferation of computation-intensive applications and smart user terminals, it is predicted that mobile data traffic will further expand by about 1000 times in the next decade [1]. Nevertheless, it will be difficult to provide the required mobile data services in remote areas due to the economic efficiency. As a complementary technology, satellite communications can overcome long distances and inhospitable terrains, provide wide coverage and achieve high data rate transmission in areas where traditional wireless infrastructure cannot be easily deployed [2]–[4]. To exploit the advantages of both terrestrial and satellite networks, the framework of satellite-terrestrial integrated networks (STIN) has been proposed for future wireless communication networks [5]–[7]. Indeed, by optimizing the utilization of wireless resources of both types of networks, this framework can enable more efficient transmission while providing flexibility in terms of user access.

Owing to the broadcast nature of wireless communications, the secure transmission of confidential information in STIN remains a serious issue. Traditionally, secure communications have been guaranteed by cryptographic techniques at upper layers of the protocol stack based on the assumption of limited computational capabilities of eavesdroppers, which is now being challenged. By exploiting properties of the wireless channels along with advanced signal processing techniques, communications can also be secured at the physical layer, which has attracted substantial research interests in recent years [8]–[10]. Transmit beamforming (BF), which can enhance received signal quality at the intended recipient while suppressing signal leakage to unintended users, and artificial jamming, which can add artificial noise at the eavesdropper without affecting the legitimate channel, have been widely studied as effective methods to realize secure communications in wireless networks [11]–[13]. However, artificial jamming is not suitable for satellite transmissions due to the long distance between the satellite and ground users, which leads to a wide coverage area on the earth surface and makes it difficult to precisely distinguish between the legitimate users and eavesdroppers. Alternatively, cooperative jamming from terrestrial networks has been studied as a means to enhance security of satellite communications in STIN, as first introduced in [14]. The authors in [15] considered a more general scenario with multiple eavesdroppers and investigated

0090-6778 © 2021 IEEE. Personal use is permitted, but republication/redistribution requires IEEE permission.
See https://www.ieee.org/publications/rights/index.html for more information.

Authorized licensed use limited to: McGill University. Downloaded on November 21,2022 at 05:36:04 UTC from IEEE Xplore. Restrictions apply.

a joint BF scheme to minimize the transmit power under secrecy constraints. By combining STIN with non-orthogonal multiple access, a joint BF and power allocation approach was introduced to solve the sum rate maximization problem in [16].

Besides, due to the huge energy consumption of base stations and especially the radio access subsystems, energy efficiency (EE) in terms of bits per second (bps) per Hertz per Joule will become an important metric from both economic and ecological perspectives for the design of future communication networks [17]. In this regard, the authors in [18] formulated a global EE maximization problem by jointly optimizing the transmit BF vectors and the AN covariance matrix in a multiple-input-single-output system. In [19], the authors presented a new perspective for the relationship between EE and spectral efficiency based on energy-efficient power control and gave insights about the EE-based performance of various transmission techniques. The authors in [20] studied the EE maximization problem for a multi-user underlay cognitive radio network, and adopted the difference of convex functions method to obtain approximate solutions.

As mentioned above, existing works mainly addressed the issues of secrecy rate maximization and EE maximization separately. As energy costs and security requirements for communications continue to rise, to achieve a better trade-off between the secrecy rate and EE, secrecy energy efficiency (SEE) has been proposed as a novel design criterion in the context of secure green communications, which is defined as the ratio between the secrecy rate and the consumed power [21]. Specifically in [21], the authors investigated the SEE maximization problem in an underlay cognitive radio network under the transmit power, secrecy rate and quality-of-service (QoS) constraints. In [22], taking both cases of instantaneous and statistical channel state information cases into account, the authors proposed secrecy energy efficiency maximization schemes and solved the approximate convex problems by using the difference of convex functions approximation approach. The authors in [23] investigated the outage-constrained SEE optimization problem in underlay energy harvesting cognitive radio networks, and utilized semi-definite relaxation, Bernstein-type inequality approach and fractional programming theory to solve the problem.

In the above-mentioned works [18]–[21], it is assumed that the channel state information (CSI) of all links is perfectly known. However, due to the mobility of terminals, estimation errors, and feedback quantization and delays, it is impossible to obtain perfect CSI [24], [25]. Therefore, robust BF design based on imperfect CSI has received considerable attention in recent years. Among the existing techniques for robust BF design, three kinds of channel uncertainty models have been used, namely: deterministic uncertainty model [26]–[28], stochastic uncertainty model [29], [30] and angular information based uncertainty model [31]–[33].[1]

The deployment of large-scale antenna array technology will become essential to achieve high antenna gain against severe path loss and provide high data rate in future wireless communication systems, especially in the millimeter wave (mmWave) spectrum. In this context, the conventional fully-digital BF designs, which require the use of one radio frequency (RF) chain per antenna, cannot be employed due to their substantial power consumption and implementation complexity. As an alternative, hybrid analog-digital BF can be exploited to achieve a sensible cost-performance trade-off [34]. In this approach, BF is realized as a cascade of two subsystems: a low-dimensional digital BF section feeding N_r RF chains, followed by an analog BF section feeding N_b antennas, where in practice, $N_r < N_b$. The analog BF section, comprised mainly of phase shifters to reduce implementation costs, allows beam steering with high gain, while the digital BF section provides additional boost in performance through precoding or other advanced signal processing (e.g., see [35] and references therein). The authors in [36] proposed a general optimization framework for hybrid analog-digital BF design in the context of STIN; however, the SEE performance metric and imperfect CSI assumption were not taken into account.

In this paper, motivated by the above considerations and the importance of SEE as a key performance metric for the evaluation of security and EE in future networks, we investigate the problem of SEE optimization in STIN with hybrid analog-digital beamforming. Our main contributions are summarized as follows:

- Considering the secure downlink transmission scenario in STIN, we adopt a uniform planar array (UPA) configuration at the BS to control both the azimuth and elevation angles of the beams and provide adequate BF gain in the coverage area. The UPA configuration can exploit three-dimensional BF schemes to improve system performance. We investigate three different hybrid BF architectures, namely: fully-connected versus partially connected with either localized or interleaved subarrays. Under imperfect knowledge of the wiretap channel angle of departure (AoD), we formulate a constrained optimization problem to maximize the SEE while satisfying the signal-to-interference-plus-noise ratio SINR) requirements of both ES and cellular users. To the best of our knowledge, the SEE maximization problem with a hybrid array is addressed for the first time in this paper whereas existing works on STIN focused on different performance criteria, e.g. [7] and [33] aimed at secrecy rate maximization, while [15] and [30] focused on the power minimization problem.
- We consider two specific scenarios with single and multiple ESs. The resulting constrained SEE optimization problems are quite challenging since the traditional digital BF design schemes [21] exploiting the Dinkelbach type algorithm [37] of fractional programming cannot be extended to the hybrid BF structure due to the coupling between the digital and analog variables. For the case of a single ES, we integrate the Charnes-Cooper approach with an iterative search algorithm to convert the original nonconvex problem into a solvable one and obtain the desired BF weight vectors. For the case of multiple ESs, by exploiting the sequential convex approximation (SCA) method, we convert the original problem into a linear one

[1]Note that part of this manuscript has been presented in [32].

Authorized licensed use limited to: McGill University. Downloaded on November 21,2022 at 05:36:04 UTC from IEEE Xplore. Restrictions apply.

with multiple linear matrix inequalities and second-order cone constraints, and obtain a solution with satisfactory performance.
- Simulation results clearly demonstrate the SEE performance advantages of the proposed hybrid BF design scheme over existing benchmark approaches. For the case of single ES, the hybrid BF scheme with localized subarrays outperforms the one with interleaved subarrays, while for the multiple ESs case, the converse is true. We believe that our proposed hybrid BF design framework can provide an effective solution to enhance the SEE of STINs.

Notation: Bold uppercase and lowercase letters denote matrices and vectors, respectively. $(\cdot)^T$, $(\cdot)^H$, $\mathrm{Tr}(\cdot)$ and $\mathrm{rank}(\cdot)$ stand for the transpose, Hermitian transpose, trace and rank of a matrix. $\|\cdot\|$ denotes the Euclidean norm of a vector, and $|\cdot|$ the magnitude of a complex scalar. $\mathbb{C}^{M\times N}$ denotes the complex space of $M\times N$ matrices. $\mathbf{I}_N$ is the $N\times N$ identity matrix. $\mathbf{X}\succeq\mathbf{0}$ represents a positive semi-definite matrix. $\mathbf{X}\odot\mathbf{Y}$ and $\mathbf{X}\otimes\mathbf{Y}$ denote the Hadamard and Kronecker products of matrices $\mathbf{X}$ and $\mathbf{Y}$, respectively, while $\langle\mathbf{X},\mathbf{Y}\rangle=\mathrm{Tr}\left(\mathbf{X}^H\mathbf{Y}\right)$. $\mathcal{CN}(\mu,\sigma^2)$ denotes the circular complex Gaussian distribution with mean μ and variance σ^2.

II. System Model and Problem Formulation

As shown in Fig. 1, we consider a cloud based STIN, where the cloud processing center (CPC), which links the satellite (SAT) gateway and the wireless BS, acts as the integrated resource management and control center of the entire network. In the STIN, the satellite and base station share the same mmWave frequency band. The geostationary orbit (GEO) satellite serves L earth stations (ESs) using unicast communications in the presence of $\sum_{l=1}^{L}K_l$ potential eavesdroppers (Eves), where K_l is the number of Eves on the l-th ES. Meanwhile, the BS serves M cellular users (CUs) using broadcast communications. Since the long distance transmission and wider earth footprint make satellite communications vulnerable and easy to intercept, not to mention the worst case scenario where the satellite legitimate and wiretap channels might be highly correlated, the utilization of physical layer security technology onboard is not efficient and also incurs an additional computational burden. To address this issue, the interference from the BS in STIN is exploited to secure the satellite downlink transmission. Thus, this paper focuses on utilizing the interference from the BS to improve the secrecy-energy efficiency performance and thereby achieve secure and efficient communications.

A. Channel Model

As illustrated in Fig. 2(a), the multibeam satellite employs an array fed reflector antenna with N_s feeds uniformly positioned along a circle with radius d plus another feed at the center of the circle [16]. To build a realistic satellite downlink channel model, the effects of path loss, rain attenuation and satellite beam gains are taken into consideration. The geometry based satellite downlink channel vector (CV) between the SAT

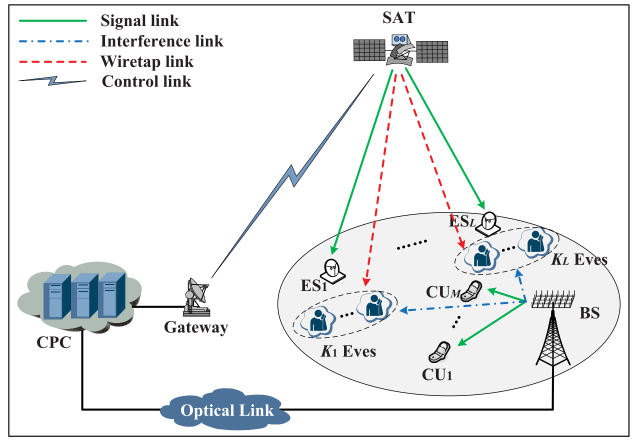

Fig. 1. System model of the considered STIN.

and any user can be expressed as [16]

$$\mathbf{f}=\sqrt{C_L G_R/\xi}\cdot\mathbf{b}_g(\phi,\psi)\odot\mathbf{a}_c(\phi,\psi) \tag{1}$$

where C_L denotes the path loss coefficient, G_R denotes the off-boresight antenna gain pattern, ξ is the rain attenuation coefficient which follows the log-normal probability distribution [38], $\mathbf{b}_g(\phi,\psi)$ denotes the vector of beam gains corresponding to the different satellite antenna feeds, with $\phi\in[0,\pi/2)$ and $\psi\in[0,2\pi)$ being the elevation angle and the azimuth angle, respectively. The array steering vector $\mathbf{a}_c\in\mathbb{C}^{N_s\times 1}$ can be expressed as

$$\mathbf{a}_c(\phi,\psi)=\left[1,e^{j\beta d\sin\phi\cos(-\psi)},\cdots,e^{j\beta d\sin\phi\cos\left(\frac{2\pi(N_s-2)}{N_s-1}-\psi\right)}\right]^T.$$

As for the terrestrial downlink transmissions, in Fig. 3(b) we assume that the BS employs a uniform planar array of dimension $N_b=N_1\times N_2$ to achieve high gain with compact size. Due to the highly directional and quasi-optical nature of mmWave transmissions, the terrestrial downlink channel can be modeled as the superposition of a predominant line-of-sight (LoS) propagation component and a sparse set of single-bounce non-LoS (NLoS) components, which is adequate for urban environments. Hence, the terrestrial downlink channel matrix can be expressed as [33]

$$\begin{aligned}\mathbf{h}=&\sqrt{g(\theta_0,\varphi_0)}\rho_0\mathbf{a}_a(\theta_0,\varphi_0)\otimes\mathbf{a}_e(\theta_0,\varphi_0)\\&+\sqrt{\frac{1}{N}}\sum_{n=1}^{N}\sqrt{g(\theta_n,\varphi_n)}\rho_n\mathbf{a}_a(\theta_n,\varphi_n)\otimes\mathbf{a}_e(\theta_n,\varphi_n)\end{aligned} \tag{2}$$

where N is the number of NLoS paths, ρ_0 and $\rho_n\,(n=1,\ldots,N)$ represent the complex channel gains associated with the LoS path and the n-th NLoS path, respectively. The gains of the NLoS components are typically 5 to 10 dB weaker than that of the LoS component based on the recent measurements in [33]. In addition, $g(\theta,\varphi)$ is the common directivity pattern of the antenna elements, with θ and φ being the vertical and horizontal AoDs, respectively. The azimuth and elevation steering vectors $\mathbf{a}_a(\theta,\varphi)\in\mathbb{C}^{N_1\times 1}$ and

Authorized licensed use limited to: McGill University. Downloaded on November 21,2022 at 05:36:04 UTC from IEEE Xplore. Restrictions apply.

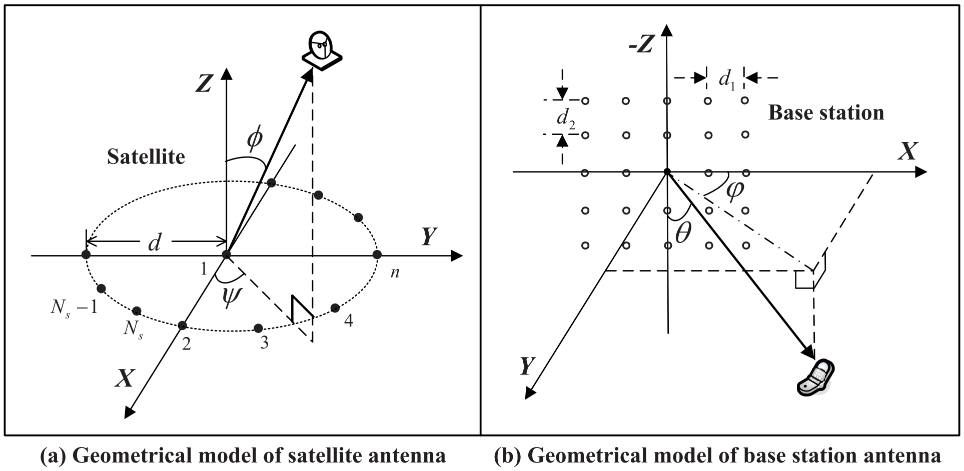

Fig. 2. Geometrical model of array antenna.

TABLE I
DESCRIPTION OF THE SYSTEM MODEL PARAMETERS

Parameter	Definition
L / M	number of ESs / CUs
N_s / N_b	antenna numbers of SAT / BS
N_1 / N_2	number of array elements along the X / Z-axis
d_1 / d_2	inter-element spacing along the X / Z-axis
$\mathbf{f}_{s,l}$ / $\mathbf{f}_{c,m}$	CV between SAT and *l*-th ES / *m*-th CU
$\mathbf{h}_{s,l}$ / $\mathbf{h}_{c,m}$	CV between BS and *l*-th ES / *m*-th CU
$\mathbf{w}_{s,l}$ / $\mathbf{w}_{c,m}$	BF weight vector toward ESs / *m*-th CU
$\sigma_{s,l}^2$ / $\sigma_{c,m}^2$	noise variance at *l*-th ES / *m*-th CU
κ / B / T	Boltzmann constant / Bandwidth / Noise temperature

$\mathbf{a}_e(\theta) \in \mathbb{C}^{N_2\times 1}$ can be expressed as

$$\begin{aligned}\mathbf{a}_a(\phi,\psi) &= \Big[1, e^{-j\beta((N_1-1)/2)d_1\sin\theta\cos\varphi},\cdots,\\ &\qquad e^{+j\beta((N_1-1)/2)d_1\sin\theta\cos\varphi}\Big]^T,\\ \mathbf{a}_e(\theta) &= \Big[e^{-j\beta((N_2-1)/2)d_2\cos\theta},\cdots,\\ &\qquad e^{+j\beta((N_2-1)/2)d_2\cos\theta}\Big]^T.\end{aligned}$$

B. Problem Formulation

Let $s_l(t)$, satisfying $E\left[|s_l(t)|^2\right]=1$, denote the information signal transmitted by the SAT to the *l*-th ES. Prior to transmission, this signal is mapped onto a BF weight vector $\mathbf{w}_l \in \mathbb{C}^{N_s\times 1}$. We emphasize that in our model, information signal $s_l(t)$ can be intercepted by anyone of the K_l Eves surrounding the *l*-th ES. Meanwhile, the BS sends a composite signal $x(t)$ with normalized power, i.e., $E\left[|x(t)|^2\right]=1$, to the CUs in its coverage area. In the current application where the BS is equipped with a large-scale (massive) antenna array, digital BF entails large system cost and complexity due to the need to use one RF chain per antenna element. To overcome this limitation, we assume that hybrid analog-digital BF is applied at the BS, where $\mathbf{P} \in \mathbb{C}^{N_b\times N_r}$ denotes the analog precoder (using only analog phase shifters) and $\mathbf{v} \in \mathbb{C}^{N_r\times 1}$ denotes the digital BF weight vector for signal $x(t)$. Other system model parameters are listed in Table I. Thus, the received signals at the *m*-th CU, *l*-th ES, and (l,k)-th Eve are, respectively, expressed as

$$\begin{aligned}y_{c,m}(t) &= \mathbf{h}_{c,m}^H\mathbf{P}\mathbf{v}x(t)+\sum_{l=1}^{L}\mathbf{f}_{c,m}^H\mathbf{w}_l s_l(t)+n_{c,m}(t),\\ y_{s,l}(t) &= \mathbf{f}_{s,l}^H\mathbf{w}_l s_l(t)+\sum_{i=1,i\neq l}^{L}\mathbf{f}_{s,l}^H\mathbf{w}_i s_i(t)\\ &\quad+\mathbf{h}_{s,l}^H\mathbf{P}\mathbf{v}x(t)+n_{s,l}(t),\\ y_{l,k}(t) &= \mathbf{f}_{l,k}^H\mathbf{w}_l s_l(t)+\sum_{i=1,i\neq l}^{L}\mathbf{f}_{l,k}^H\mathbf{w}_i s_i(t)\\ &\quad+\mathbf{h}_{l,k}^H\mathbf{P}\mathbf{v}x(t)+n_{l,k}(t)\end{aligned}\tag{3}$$

where $n_{c,m}(t), n_{s,l}(t)$ and $n_{l,k}(t)$ denote i.i.d. complex Gaussian random noises with variance $\sigma^2=\kappa BT$. The received SINR at the *m*-th CU, *l*-th ES, and (l,k)-th Eve can be written as

$$\begin{aligned}\gamma_{c,m} &= \frac{\left|\mathbf{h}_{c,m}^H\mathbf{P}\mathbf{v}\right|^2}{\sum\limits_{l=1}^{L}\left|\mathbf{f}_{c,m}^H\mathbf{w}_l\right|^2+\sigma^2},\\ \gamma_{s,l} &= \frac{\left|\mathbf{f}_{s,l}^H\mathbf{w}_l\right|^2}{\sum\limits_{i=1,i\neq l}^{L}\left|\mathbf{f}_{s,l}^H\mathbf{w}_i\right|^2+\left|\mathbf{h}_{s,l}^H\mathbf{P}\mathbf{v}\right|^2+\sigma^2},\\ \gamma_{l,k} &= \frac{\left|\mathbf{f}_{l,k}^H\mathbf{w}_l\right|^2}{\sum\limits_{i=1,i\neq l}^{L}\left|\mathbf{f}_{l,k}^H\mathbf{w}_i\right|^2+\left|\mathbf{h}_{l,k}^H\mathbf{P}\mathbf{v}\right|^2+\sigma^2}.\end{aligned}\tag{4}$$

Therefore, the achievable secrecy rate of the *l*-th ES is given by

$$R_{s,l}=\left[\log_2(1+\gamma_{s,l})-\max_{k\in\{1,\cdots,K_l\}}\log_2(1+\gamma_{l,k})\right]^+\tag{5}$$

Authorized licensed use limited to: McGill University. Downloaded on November 21,2022 at 05:36:04 UTC from IEEE Xplore. Restrictions apply.

where $[x]^+ = \max(x,0)$. Total power consumption P_{tot} of the considered system is modeled as

$$\begin{aligned} P_{tot} &= \eta_1 \sum_{l=1}^{L} \|\mathbf{w}_l\|^2 + \eta_2 \|\mathbf{v}\|^2 + P_S + P_B, \\ P_S &= N_s (P_{sr} + P_{sa}) + P_{sb}, \\ P_B &= N_r (P_{br} + P_{bs}) + N_b (P_{ba} + c P_{bp}) + P_{bb} \end{aligned} \tag{6}$$

where $\eta_1 > 1$ and $\eta_2 > 1$ are constants which account for the power amplifier inefficiency of the satellite and BS, respectively. P_{bp} and P_{bs} denote the power consumption of the phase shifters and power splitters, respectively, while P_{sr} and P_{br}, P_{sa} and P_{ba}, P_{sb} and P_{bb} represent the power consumed by the RF chains, power amplifiers, and baseband processor of the satellite and BS, respectively [39]. The parameter c is equal to N_r for the fully-connected architecture and to 1 for the sub-array architecture.

In practice, due to the mobility of terminals and estimation mismatch of the wiretap CSI, perfect knowledge of the wiretap CSI is unavailable. Considering the high directionality of the mmWave channel, the angular information based uncertainty model has been exploited in STIN [33]. Thus, we assume that only imperfect knowledge of the AoD for the wiretap CSI is available at the BS [25]. Specifically, the channel from BS to the k-th Eve $\mathbf{h}_{l,k}$ belongs to a given AoD uncertainty set $\Delta_{l,k}$ specified by $\theta_{l,k} \in \left[\theta_{l,k}^L, \theta_{l,k}^U\right]$ and $\varphi_{l,k} \in \left[\varphi_{l,k}^L, \varphi_{l,k}^U\right]$, which is also applicable to the satellite wiretap channels $\mathbf{f}_{l,k}$.

In this paper, we aim to maximize the secrecy-energy efficiency, defined as the ratio of the achievable sum rate to the total power consumption, while satisfying the SINR requirements of the ESs and CUs, analog precoder modula constraint and transmit power constraints. Mathematically, the optimization problem can be formulated as

$$\max_{\mathbf{w}_l, \mathbf{v}, \mathbf{P}} \ \sum\nolimits_{l=1}^{L} \mu_l R_{s,l} / P_{tot} \tag{7a}$$

$$\text{s.t } \gamma_{c,m} \geq \Gamma_c, \quad \forall m, \tag{7b}$$

$$\gamma_{s,l} \geq \Gamma_s, \quad \forall l, \tag{7c}$$

$$\left|[\mathbf{P}]_{i,j}\right|^2 = a_{i,j}, \quad i = 1, \cdots, N_b, \ j = 1, \cdots, N_r, \tag{7d}$$

$$\|\mathbf{v}\|_F^2 \leq P_b, \quad \|\mathbf{w}_l\|_F^2 \leq P_{s,l}, \ \forall l \tag{7e}$$

where μ_l is the positive weighting factor assigned to the l-th ES, Γ_c and Γ_s denote the SINR thresholds of the CUs and ESs, respectively, P_b and $P_{s,l}$ are the power budget of the CUs and l-th ES. The value of $a_{i,j}$ in (7d) depends on the hybrid array structure as follows

$$\left|[\mathbf{P}]_{i,j}\right|^2 = \begin{cases} 1/N_b, & \text{Full-array,} \\ \left[a \ \mathbf{1}_{N_b/N_r} \otimes \mathbf{I}_{N_r}\right]_{i,j}, & \text{Interleaved,} \\ \left[a \ \mathbf{I}_{N_r} \otimes \mathbf{1}_{N_b/N_r}\right]_{i,j}, & \text{Localized.} \end{cases} \tag{8}$$

where $a = N_r/N_b$ and $\mathbf{1}_{N_b/N_r}$ denotes a vector with N_b/N_r elements equal to 1.

Fig. 3 illustrates four typical beamforming architectures in mmWave systems, namely: (a) the fully-digital beamforming architecture; (b) the fully-connected hybrid beamforming architecture; (c) the localized sub-array hybrid beamforming architectures; and (d) the interleaved sub-array hybrid beamforming architecture. Clearly, the fully-digital beamforming architecture uses $N_r = N_b$ RF chains, and thus achieves better spectral efficiency with increasing computational burden and RF power consumption. The fully-connected hybrid beamforming architecture can achieve a better trade-off between spectral efficiency and power consumption due to the use of less RF chains, but its analog part with additional $N_r N_b$ phase shifters is also difficult to implement. Thus, to complement the fully-connected architecture, two sub-array architectures, called localized array and interleaved array are investigated, where in the former, antenna elements are adjacent to each other, while in the latter antenna elements are uniformly placed in each sub-array [40].

Here, we discuss the technical challenges facing the solution of the problem described above. Firstly, we consider the digital BF scheme, which has been widely used to solve EE and SEE maximization problems [22]. It can be verified that, by assuming that $N_r = N_b$ and $[\mathbf{P}]_{i,j} = [\mathbf{b} \otimes \mathbf{I}_{N_r}]_{i,j}, \mathbf{b} = (1, 0, \cdots, 0)^T$, the above hybrid BF optimization problem corresponds to a more general form of the digital BF optimization problem. However, the existing schemes for the design of digital BF cannot be directly extended to solving the above complex problem due to the nonconvex objective function with coupled optimization variables, and the nonconvex constraints on the elements of the analog precoder and combiners. Secondly, the difference between the hybrid architectures in Fig. 3(b)-(d) lies in the different constraints imposed on the analog precoder, and it is obvious that the fully-connected architecture would achieve better SE with increasing computational burden than the localized and interleaved sub-array architectures. Here, we will investigate the optimal BF scheme defined by (7) for the three hybrid architectures through transformations of the non-convex analog precoder constraints. Thirdly, since the hybrid architectures based SEE maximization problem with a single ES (surrounded by multiple Eves) has not been investigated in the literature, we will first investigate the above optimization problem with $L = 1$, and exploit the Charnes-Cooper approach combined with an iterative algorithm to convert the original nonconvex problem into a solvable one and obtain the BF weight vectors. Then, we will investigate the multiple ESs scenario, and adopt the sequential convex approximation method to convert the original problem into a linear one with a series of linear matrix inequalities and second-order cone constraints, and obtain the solutions.

III. Hybrid Beamforming for Single ES

In this section, we propose a low-complexity hybrid beamforming scheme to solve the optimization problem (19) for the single ES scenario ($L = 1$).

A. Discretization Method for Approximating Imperfect AoD

Since the objective function (7a) is non-convex due to the imperfect wiretap CSI model with infinite possibilities, we exploit a discretization method to convert the imperfect

Authorized licensed use limited to: McGill University. Downloaded on November 21,2022 at 05:36:04 UTC from IEEE Xplore. Restrictions apply.

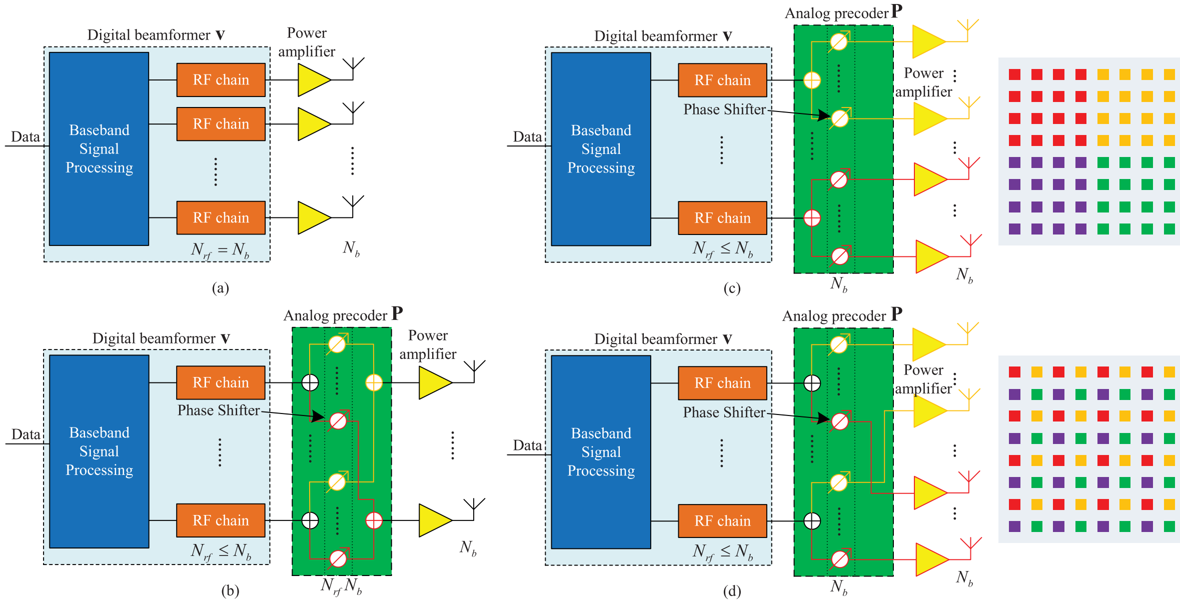

Fig. 3. Architecture comparison: (a) fully-digital architecture; (b) fully-connected hybrid architecture; (c) localized sub-array hybrid architecture; (d) interleaved sub-array hybrid architecture. The differently colored squares on the right-hand side of parts (c) and (d) are used to illustrate the different types of sub-array architectures for the UPA.

wiretap CSI into a tractable form. Specifically, the available wiretap channels belong to a given AoD uncertainty set specified by $\theta_{l,k} \in \left[\theta_{l,k}^L, \theta_{l,k}^U\right], \varphi_{l,k} \in \left[\varphi_{l,k}^L, \varphi_{l,k}^U\right]$, and we select uniformly spaced angles as

$$\begin{aligned} \theta_{l,k}^{(i)} &= \theta_{l,k}^L + (i-1)\,\Delta\theta, \quad i = 1, \cdots, M_1, \\ \varphi_{l,k}^{(j)} &= \varphi_{l,k}^L + (j-1)\,\Delta\varphi, \quad j = 1, \cdots, M_2 \end{aligned} \tag{9}$$

where $\theta_{l,k}^{(i)}$ and $\varphi_{l,k}^{(j)}$ are the elevation and azimuth AoD, $\Delta\theta = (\theta_{l,k}^U - \theta_{l,k}^L)/(M_1-1)$ and $\Delta\varphi = (\varphi_{l,k}^U - \varphi_{l,k}^L)/(M_2-1)$. The above formulation is also suitable for the satellite downlink channel by replacing θ and φ with ϕ and ψ, which is omitted for brevity. Then, we define $\tilde{\mathbf{H}} = \sum_{i=1}^{M_1}\sum_{j=1}^{M_2} \mu_{i,j}\mathbf{H}^{(i,j)}$ and $\tilde{\mathbf{F}} = \sum_{i=1}^{M_1}\sum_{j=1}^{M_2} \mu_{i,j}\mathbf{F}^{(i,j)}$, where $\mathbf{H}^{(i,j)} = \mathbf{h}^{(i,j)}\left(\mathbf{h}^{(i,j)}\right)^H$ and $\mathbf{F}^{(i,j)} = \mathbf{f}^{(i,j)}\left(\mathbf{f}^{(i,j)}\right)^H$ and $\mu_{i,j} = \frac{1}{M_1 M_2}$. This discretization method has been adopted in [29] with satisfactory robustness.

Remark 1: Assuming that the satellite uses a multibeam antenna and the BS employs a UPA with hybrid digital-analog architecture, we formulate a joint optimization problem to maximize the SEE subject to the SINR requirement of ESs and CUs, analog precoder modulus constraints and transmit power constraints. To the best of our knowledge, this optimization problem is formulated and solved for the first time in this paper.

B. Iterative Optimization Over $\mathbf{w}_1$, $\mathbf{v}$ and $\mathbf{P}$

It can be observed that the optimization problem (7) is coupled in the variables $\mathbf{v}$ and $\mathbf{P}$, which makes it intractable. In order to solve this non-convex problem, we propose an optimization scheme to iteratively solve the digital and analog BF weight vectors.

First, we investigate optimization of the digital BF weight vector. While the objective function of (7a) is mathematically intractable due to the fractional form of SEE, by introducing auxiliary α and τ into problem (7), it can be transformed as

$$\max_{\mathbf{W}_1,\mathbf{V},\mathbf{P}} \quad \tau^{-1}\log_2\left(\frac{\sigma^2+\mathrm{Tr}\left(\mathbf{F}_{s,1}\mathbf{W}_1\right)+\mathrm{Tr}\left(\mathbf{P}^H\mathbf{H}_{s,1}\mathbf{P}\mathbf{V}\right)}{\alpha}\right) \tag{10a}$$

$$\text{s.t.} \ \eta_1\mathrm{Tr}\left(\mathbf{W}_1\right)+\eta_2\mathrm{Tr}\left(\mathbf{V}\right)+P_S+P_B=\tau, \tag{10b}$$

$$\frac{\mathrm{Tr}\left(\tilde{\mathbf{F}}_{1,k}\mathbf{W}_1\right)\left(\mathrm{Tr}\left(\mathbf{P}^H\mathbf{H}_{s,1}\mathbf{P}\mathbf{V}\right)+\sigma^2\right)}{\mathrm{Tr}\left(\mathbf{P}^H\tilde{\mathbf{H}}_{1,k}\mathbf{P}\mathbf{V}\right)+\sigma^2} \leq \alpha, \quad \forall k, \tag{10c}$$

$$\mathrm{Tr}\left(\mathbf{P}^H\mathbf{H}_{c,m}\mathbf{P}\mathbf{V}\right)-\Gamma_c\left(\mathrm{Tr}\left(\mathbf{F}_{c,m}\mathbf{W}_1\right)+\sigma^2\right) \geq 0, \quad \forall m, \tag{10d}$$

$$\mathrm{Tr}\left(\mathbf{F}_{s,1}\mathbf{W}_1\right)-\Gamma_s\left(\mathrm{Tr}\left(\mathbf{P}^H\mathbf{H}_{s,1}\mathbf{P}\mathbf{V}\right)+\sigma^2\right) \geq 0, \tag{10e}$$

$$\left|[\mathbf{P}]_{i,j}\right|^2 = \beta_{i,j}, i=1,\cdots,N_b, \quad j=1,\cdots,N_r, \tag{10f}$$

$$\mathrm{Tr}\left(\mathbf{W}_1\right) \leq P_{s,1}, \quad \mathrm{Tr}\left(\mathbf{V}\right) \leq P_b, \tag{10g}$$

$$\mathrm{rank}\left(\mathbf{W}_1\right)=1, \quad \mathrm{rank}\left(\mathbf{V}\right)=1. \tag{10h}$$

where $\mathbf{W}_1 = \mathbf{w}_1\mathbf{w}_1^H$, $\mathbf{V} = \mathbf{v}\mathbf{v}^H$.

Suppose that after the n-th iteration, we have obtained an analog precoder $\mathbf{P}^{(n)}$. Then, the optimization problem for the digital beamformer can be expressed as

$$\max_{\mathbf{W}_1,\mathbf{V},\tau,\alpha} \quad \tau^{-1}\log_2\left(\frac{x+\mathrm{Tr}\left(\mathbf{P}^{(n)H}\mathbf{H}_{s,1}\mathbf{P}^{(n)}\mathbf{V}\right)}{\alpha}\right) \tag{11a}$$

$$\text{s.t.} \ \eta_1\mathrm{Tr}\left(\mathbf{W}_1\right)+\eta_2\mathrm{Tr}\left(\mathbf{V}\right)+P_S+P_B=\tau, \tag{11b}$$

Authorized licensed use limited to: McGill University. Downloaded on November 21,2022 at 05:36:04 UTC from IEEE Xplore. Restrictions apply.

$$\frac{\mathrm{Tr}\left(\tilde{\mathbf{F}}_{1,k}\mathbf{W}_1\right)\left(\mathrm{Tr}\left(\mathbf{P}^{(n)H}\mathbf{H}_{s,1}\mathbf{P}^{(n)}\mathbf{V}\right)+\sigma^2\right)}{\mathrm{Tr}\left(\mathbf{P}^{(n)H}\tilde{\mathbf{H}}_{1,k}\mathbf{P}^{(n)}\mathbf{V}\right)+\sigma^2}\leq\alpha,\quad \forall k, \tag{11c}$$

$$\mathrm{Tr}\left(\mathbf{P}^{(n)H}\mathbf{H}_{c,m}\mathbf{P}^{(n)}\mathbf{V}\right)-y\Gamma_c\geq 0,\quad\forall m, \tag{11d}$$

$$\mathrm{Tr}\left(\mathbf{F}_{s,1}\mathbf{W}_1\right)-\Gamma_s\left(\mathrm{Tr}\left(\mathbf{P}^{(n)H}\mathbf{H}_{s,1}\mathbf{P}^{(n)}\mathbf{V}\right)+\sigma^2\right)\geq 0, \tag{11e}$$

$$\mathrm{Tr}\left(\mathbf{W}_1\right)\leq P_{s,1},\quad \mathrm{Tr}\left(\mathbf{V}\right)\leq P_b, \tag{11f}$$

$$\mathrm{rank}\left(\mathbf{W}_1\right)=1,\quad \mathrm{rank}\left(\mathbf{V}\right)=1. \tag{11g}$$

where $x = \sigma^2 + \mathrm{Tr}\left(\mathbf{F}_{s,1}\mathbf{W}_1\right)$, $y = \mathrm{Tr}\left(\mathbf{F}_{c,m}\mathbf{W}_1\right)+\sigma^2$. To make the above nonconvex problem (11) solvable, we propose a two-stage optimization algorithm for solving (11), where the outer problem can be written as

$$\begin{aligned}&\max_{\tau}\ \tau^{-1}f\left(\tau\right)\\&\text{s.t. }\tau\in\left[P_S+P_B,\eta_1P_{s,1}+\eta_2P_b+P_S+P_B\right]\end{aligned} \tag{12}$$

where $f\left(\tau\right)=\log_2\left(\sigma^2+\mathrm{Tr}\left(\mathbf{F}_{s,1}\mathbf{W}_1\right)/\alpha\right)$. Since $\log_2\left(\cdot\right)$ is monotonically increasing, the latter problem can be expressed as

$$\begin{aligned}&\max_{\mathbf{W}_1,\mathbf{V},\alpha}\ \frac{\sigma^2+\mathrm{Tr}\left(\mathbf{F}_{s,1}\mathbf{W}_1\right)+\mathrm{Tr}\left(\mathbf{P}^{(n)H}\mathbf{H}_{s,1}\mathbf{P}^{(n)}\mathbf{V}\right)}{\alpha}\\&\text{s.t. }(11b)-(11g).\end{aligned} \tag{13}$$

Obviously, the outer problem can be solved by one-dimensional search (such as the bisection method) on τ in the interval $[P_S+P_B,\eta_1P_{s,1}+\eta_2P_b+P_S+P_B]$. Then, we adopt the Charnes-Cooper approach to solve the inner optimization problem. By introducing variables $\beta = 1/\alpha$, and assuming $\bar{\mathbf{W}}_1 = \mathbf{W}_1/\alpha$ and $\bar{\mathbf{V}} = \mathbf{V}/\alpha$, the inner optimization problem can be expressed as

$$\max_{\bar{\mathbf{W}}_1,\ \bar{\mathbf{V}},\beta}\beta\sigma^2+\mathrm{Tr}\left(\mathbf{F}_{s,1}\bar{\mathbf{W}}_1\right)+\mathrm{Tr}\left(\mathbf{P}^{(n)H}\mathbf{H}_{s,1}\mathbf{P}^{(n)}\bar{\mathbf{V}}\right) \tag{14a}$$

$$\text{s.t. }\eta_1\mathrm{Tr}\left(\bar{\mathbf{W}}_1\right)+\eta_2\mathrm{Tr}\left(\bar{\mathbf{V}}\right)=\left(\tau-P_S-P_B\right)\beta, \tag{14b}$$

$$f_1\leq\mathrm{Tr}\left(\mathbf{P}^{(n)H}\tilde{\mathbf{H}}_{1,k}\mathbf{P}^{(n)}\bar{\mathbf{V}}\right)+\beta\sigma^2,\quad\forall k, \tag{14c}$$

$$\mathrm{Tr}\left(\mathbf{P}^{(n)H}\mathbf{H}_{c,m}\mathbf{P}^{(n)}\bar{\mathbf{V}}\right)-y\Gamma_c\geq 0,\quad\forall m, \tag{14d}$$

$$\mathrm{Tr}\left(\mathbf{F}_{s,1}\bar{\mathbf{W}}_1\right)-\Gamma_s\sigma^2\beta\geq 0, \tag{14e}$$

$$\mathrm{Tr}\left(\bar{\mathbf{W}}_1\right)\leq P_{s,1}\beta,\quad\mathrm{Tr}\left(\bar{\mathbf{V}}\right)\leq P_b\beta, \tag{14f}$$

$$\mathrm{rank}\left(\bar{\mathbf{W}}_1\right)=1,\quad\mathrm{rank}\left(\bar{\mathbf{V}}\right)=1 \tag{14g}$$

where $f_1 = \mathrm{Tr}\left(\tilde{\mathbf{F}}_{1,k}\bar{\mathbf{W}}_1\right)\left(\mathrm{Tr}\left(\mathbf{P}^{(n)H}\mathbf{H}_{s,1}\mathbf{P}^{(n)}\bar{\mathbf{V}}\right)+\beta\sigma^2\right)$. To deal with the nonconvex constraint (14c), we introduce an auxiliary variable υ which allows to transform (14c) into a second-order cone (SOC) as follows

$$\begin{aligned}\frac{\mathrm{Tr}\left(\tilde{\mathbf{F}}_{1,k}\bar{\mathbf{W}}_1\right)+c}{2}&\leq\left\|\left[\frac{\mathrm{Tr}\left(\tilde{\mathbf{F}}_{1,k}\bar{\mathbf{W}}_1\right)-c}{2},\upsilon\right]\right\|_2\\\frac{d+1}{2}&\geq\left\|\left[\frac{d-1}{2},\upsilon\right]^T\right\|_2\end{aligned} \tag{15}$$

where $c = \mathrm{Tr}\left(\mathbf{P}^{(n)H}\mathbf{H}_{s,1}\mathbf{P}^{(n)}\bar{\mathbf{V}}\right)+\beta\sigma^2$ and $d = \mathrm{Tr}\left(\mathbf{P}^{(n)H}\tilde{\mathbf{H}}_{1,k}\mathbf{P}^{(n)}\bar{\mathbf{V}}\right)+\beta\sigma^2$. Consequently, problem (14) is convex except for the rank-1 constraints (14g), and can be solved using semi definite relaxation (SDR) and randomization as reported in [26].

Next, we focus on solving for the analog precoder $\mathbf{P}$. Once the solution of (14) $\{\mathbf{w}_1^{(n)},\mathbf{v}^{(n)}\}$ is obtained, it will be used for finding the analog precoder. Since P_{tot} becomes constant with known $\{\mathbf{w}_1^{(n)},\mathbf{v}^{(n)}\}$, the optimization problem for the analog precoder can be written as follows

$$\begin{aligned}\max_{\mathbf{P}}\min_{k\in\{1,\cdots,K_1\}}\ &\frac{\left|\mathbf{h}_{s,1}^H\mathbf{P}\mathbf{v}^{(n)}\right|^2+\left|\mathbf{f}_{s,1}^H\mathbf{w}_1^{(n)}\right|^2+\sigma^2}{\left|\mathbf{h}_{s,1}^H\mathbf{P}\mathbf{v}^{(n)}\right|^2+\sigma^2}\cdot\frac{\left|\mathbf{h}_{1,k}^H\mathbf{P}\mathbf{v}^{(n)}\right|^2+\sigma^2}{\left|\mathbf{h}_{1,k}^H\mathbf{P}\mathbf{v}^{(n)}\right|^2+\left|\mathbf{f}_{1,k}^H\mathbf{w}_1^{(n)}\right|^2+\sigma^2}\\\text{s.t. }&\frac{\left|\mathbf{h}_{c,m}^H\mathbf{P}\mathbf{v}^{(n)}\right|^2}{\left|\mathbf{f}_{c,m}^H\mathbf{w}_1^{(n)}\right|+\sigma^2}\geq\Gamma_c,\quad\forall m,\\&\frac{\left|\mathbf{f}_{s,1}^H\mathbf{w}_1^{(n)}\right|^2}{\left|\mathbf{h}_{s,1}^H\mathbf{P}\mathbf{v}^{(n)}\right|^2+\sigma^2}\geq\Gamma_s,\\&\left|[\mathbf{P}]_{i,j}\right|^2=\beta_{i,j},i=1,\cdots,N_b,\quad j=1,\cdots,N_r.\end{aligned} \tag{16}$$

It is noted that the constraints (7c) and (7e) can be removed because $\{\mathbf{w}_1^{(n)},\mathbf{v}^{(n)}\}$ always satisfy them. Then, (16) can be re-written in the following vector form for compactness

$$\begin{aligned}\max_{\mathbf{p}}\min_{k\in\{1,\cdots,K_1\}}\ &\frac{\left|\mathbf{h}_{s,1}^H\hat{\mathbf{V}}^{(n)}\mathbf{p}\right|^2+\left|\mathbf{f}_{s,1}^H\mathbf{w}_1^{(n)}\right|^2+\sigma^2}{\left|\mathbf{h}_{s,1}^H\hat{\mathbf{V}}^{(n)}\mathbf{p}\right|^2+\sigma^2}\cdot\frac{\left|\tilde{\mathbf{h}}_{1,k}^H\hat{\mathbf{V}}^{(n)}\mathbf{p}\right|^2+\sigma^2}{\left|\tilde{\mathbf{h}}_{1,k}^H\hat{\mathbf{V}}^{(n)}\mathbf{p}\right|^2+\left|\tilde{\mathbf{f}}_{1,k}^H\mathbf{w}_1^{(n)}\right|^2+\sigma^2}\\\text{s.t. }&\left|\mathbf{h}_{c,m}^H\hat{\mathbf{V}}^{(n)}\mathbf{p}\right|^2\geq\Gamma_c\left(\left|\mathbf{f}_{c,m}^H\mathbf{w}_1^{(n)}\right|^2+\sigma^2\right),\quad\forall m,\\&\left|\mathbf{h}_{s,1}^H\hat{\mathbf{V}}^{(n)}\mathbf{p}\right|^2\leq\left|\mathbf{f}_{s,1}^H\mathbf{w}_1^{(n)}\right|^2/\Gamma_s-\sigma^2\\&\left|[\mathbf{p}]_q\right|^2=\mathrm{vec}(\Phi)_q,\quad q=1,\cdots,N_bN_r\end{aligned} \tag{17}$$

where $\hat{\mathbf{V}}^{(n)}$ = block-diag $\left(\mathbf{v}^{(n)T},\cdots,\mathbf{v}^{(n)T}\right)\in\mathbb{C}^{N_b\times N_bN_r}$, $\mathbf{p}=\mathrm{vec}\left(\mathbf{P}\right)\in\mathbb{C}^{N_bN_r\times 1}$, and matrix $\Phi\in\mathbb{C}^{N_b\times N_r}$ represents different array structures. The three hybrid structures, i.e., fully-connected, localized sub-array and interleaved sub-array, respectively, can be represented in terms of Φ as

$$\begin{aligned}\Phi_{\text{full}}&=\mathbf{1}_{N_b\times N_r}/N_b,\\\Phi_{\text{local}}&=a\ \text{block-diag}\left(\mathbf{1}_{1/a},\cdots,\mathbf{1}_{1/a}\right),\\\Phi_{\text{intr}}&=a\ \text{block-diag}\left(\mathbf{I}_{1/a},\cdots,\mathbf{I}_{1/a}\right),\end{aligned}$$

where block-diag$\left(\cdot\right)$ denotes a function and has been defined in [36], $\mathbf{1}_{N_b\times N_r}\in\mathbb{C}^{N_b\times N_r}$ denotes the all-ones matrix, $\mathbf{1}_{1/a}$ denotes the all-ones vector with size $1/a$.

Authorized licensed use limited to: McGill University. Downloaded on November 21,2022 at 05:36:04 UTC from IEEE Xplore. Restrictions apply.

Then, by introducing variable t_1, after some manipulations, problem (17) can be transformed as

$$\begin{aligned}
&\max_{\hat{\mathbf{P}},t_1}\ t_1\\
&\text{s.t.}\ \left\|\begin{bmatrix}\sqrt{\frac{t_1}{t_1-1}}\mathrm{Tr}\left(\tilde{\mathbf{F}}_{s,k}\mathbf{W}_1^{(n)}\right)\\ \frac{1}{2}\left(A-B\right)\end{bmatrix}\right\|_2\le\frac{1}{2}\left(A+B\right),\quad\forall k,\\
&\quad\mathrm{Tr}\left(\hat{\mathbf{V}}^{(n)H}\tilde{\mathbf{H}}_{c,m}\hat{\mathbf{V}}^{(n)}\hat{\mathbf{P}}\right)\\
&\quad\ge\Gamma_c\left(\mathrm{Tr}\left(\mathbf{F}_{c,m}\mathbf{W}_1^{(n)}\right)+\sigma^2\right),\quad\forall m,\\
&\quad\mathrm{Tr}\left(\hat{\mathbf{V}}^{(n)H}\mathbf{H}_{s,1}\hat{\mathbf{V}}^{(n)}\hat{\mathbf{P}}\right)\le\mathrm{Tr}\left(\mathbf{F}_{s,1}\mathbf{W}_1^{(n)}\right)/\Gamma_s-\sigma^2,\\
&\quad\mathrm{diag}\left[\hat{\mathbf{P}}\right]_q=\left[\mathbf{q}\mathbf{q}^H\right]_q,\quad q=1,\cdots,N_bN_r,\\
&\quad\mathrm{rank}\left(\hat{\mathbf{P}}\right)=1
\end{aligned}\tag{18}$$

where

$$A=\mathrm{Tr}\left(\mathbf{F}_{s,1}\mathbf{W}_1^{(n)}\right)+(1-t_1)\left(\mathrm{Tr}\left(\hat{\mathbf{V}}^{(n)H}\mathbf{H}_{s,1}\hat{\mathbf{V}}^{(n)}\hat{\mathbf{P}}\right)+\sigma^2\right)$$

$$B=\mathrm{Tr}\left(\hat{\mathbf{V}}^{(n)H}\tilde{\mathbf{H}}_{1,k}\hat{\mathbf{V}}^{(n)}\hat{\mathbf{P}}\right)+\sigma^2-\left(\frac{t_1}{t_1-1}\right)\mathrm{Tr}\left(\tilde{\mathbf{F}}_{1,k}\mathbf{W}_1^{(n)}\right)$$

and $\tilde{\mathbf{F}}_{s,k}=\mathbf{f}_{s,1}\tilde{\mathbf{f}}_{1,k}^H$, $\hat{\mathbf{P}}=\mathbf{p}\mathbf{p}^H$, $\mathbf{q}=\mathrm{vec}\left(\Phi\right)$. It is observed that the above problem can be solved by fixing the value of t_1, and thus, a bisection search over t_1, SDR and randomization method can be used to solve the problem (18). However, considering that the solution candidates from the SDR approach cannot guarantee an optimal solution for the original rank-1 constrained problem, the selected rank-1 solution may be suboptimal or even far from the optimal one. In the next subsection, we will discuss how to convert the rank-1 constraint into a convex one.

C. Non-Smooth Method

Since the SDR method does not achieve an optimal solution of problem (18), as it does not enforce the rank-1 constraint, we adopt the following iterative penalty function approach. Due to space limitations, we only consider the digital beamformer optimization in (14), but the steps for obtaining the analog precoder are similar.

Proposition 1: The non-convex optimization (18) can be equivalently transformed to the following convex optimization problem

$$\begin{aligned}
\max_{\bar{\mathbf{W}}_1,\bar{\mathbf{V}},\beta}\ &\beta\sigma^2+\mathrm{Tr}\left(\mathbf{F}_{s,1}\bar{\mathbf{W}}_1\right)\\
&-\mu_1\left(\mathrm{Tr}\left(\bar{\mathbf{W}}_1\right)-\left\langle\bar{\mathbf{w}}_{1\max}^{(n)}\bar{\mathbf{w}}_{1\max}^{(n)H},\bar{\mathbf{W}}_1\right\rangle\right)\\
&-\mu_v\left(\mathrm{Tr}\left(\bar{\mathbf{V}}\right)-\left\langle\bar{\mathbf{v}}_{\max}^{(n)}\bar{\mathbf{v}}_{\max}^{(n)H},\bar{\mathbf{V}}\right\rangle\right)\\
\text{s.t.}\ &(14b),(14d)-(14f),(15).
\end{aligned}\tag{19}$$

Proof: See Appendix.

Finally, the proposed hybrid BF design scheme with $L=1$ is summarized in Algorithm 1.

IV. Hybrid Beamforming for Multiple ESs

In the case of multiple ESs, the sum of logarithmic functions increases the optimization complexity, and the hybrid scheme

Algorithm 1: The Proposed Hybrid Scheme With $L=1$

Input: $\{\mathbf{h}_{c,m},\mathbf{h}_{1,k},\mathbf{f}_{1,k}\}$, $\mathbf{f}_{s,1}$, Γ_c, Γ_s, P_b and $P_{s,1}$.

1 Set the tolerance of accuracy ε_1 and ε_2;
2 Obtain the feasible precoder $\mathbf{P}^{(0)}$ based on (10f) ;
3 Set the iteration number $n_1=0$, $n_2=0$;
4 **repeat**
5 Initialize $\bar{\mathbf{W}}_1^{(n_2)}$ and $\bar{\mathbf{V}}^{(n_2)}$;
6 **while** $\mathrm{Tr}\left(\bar{\mathbf{W}}_1^{(n_2)}\right)-\lambda_{\max}\left(\bar{\mathbf{W}}_1^{(n_2)}\right)\ge\varepsilon_2$ *or* $\mathrm{Tr}\left(\bar{\mathbf{V}}^{(n_2)}\right)-\lambda_{\max}\left(\bar{\mathbf{V}}^{(n_2)}\right)\ge\varepsilon_2$ **do**
7 Solve the problem (19);
8 Obtain solutions $\bar{\mathbf{W}}_1$ and $\bar{\mathbf{V}}$, set $\bar{\mathbf{W}}_1^{(n_2+1)}:=\bar{\mathbf{W}}_1$ and $\bar{\mathbf{V}}^{(n_2+1)}:=\bar{\mathbf{V}}$;
9 **if** $\bar{\mathbf{W}}_1^{(n_2+1)}\approx\bar{\mathbf{W}}_1^{(n_2)}$ & $\bar{\mathbf{V}}^{(n_2+1)}\approx\bar{\mathbf{V}}^{(n_2)}$ **then**
10 Set $\eta:=2\eta$;
11 **else**
12 Set $n_2:=n_2+1$;
13 **end**
14 **end**
15 Using singular value decomposition to obtain $\mathbf{w}_1$ and $\mathbf{v}$ from solutions $\bar{\mathbf{W}}_1$, $\bar{\mathbf{V}}$;
16 Set $n_2:=0$, $\mathbf{w}_1^{(n_1+1)}=\mathbf{w}_1,\mathbf{v}^{(n_1+1)}=\mathbf{v}$;
17 Compute $\mathbf{P}^{(n_1+1)}$ through nonsmooth method on problem (18) with similar procedure of *step* 5-16;
18 Set $n_1:=n_1+1$;
19 **until** $\left|\mathbf{P}^{(n_1)}\mathbf{v}^{(n_1)}-\mathbf{P}^{(n_1-1)}\mathbf{v}^{(n_1-1)}\right|^2\le\varepsilon_1$;

Output: Analog precoder $\mathbf{P}$, digital beamformers $\mathbf{w}_1$, $\mathbf{v}$.

for single ES cannot be used to solve this problem. Here, we propose a hybrid scheme by exploiting the SCA method to solve the complex non-convex problem. Firstly, by introducing the positive auxiliary variables $\{x_l,y_l,p_l,q_l\}$ into the objective function (7a), problem (7) can be rewritten as

$$\max_{\substack{\mathbf{P},\mathbf{w}_l,\mathbf{v},\\x_l,y_l,p_l,q_l}}\ \frac{\sum_{l=1}^{L}\mu_l\left(x_l-y_l-p_l+q_l\right)}{\eta_1\sum_{l=1}^{L}\|\mathbf{w}_l\|^2+\eta_2\|\mathbf{v}\|^2+P_S+P_B}\tag{20a}$$

$$\text{s.t.}\ \sum_{j=1}^{L}\left|\mathbf{f}_{s,l}^H\mathbf{w}_j\right|^2+\left|\mathbf{h}_{s,l}^H\mathbf{P}\mathbf{v}\right|^2+\sigma^2\ge e^{x_l},\quad\forall l,\tag{20b}$$

$$\sum_{i\neq l}^{L}\left|\mathbf{f}_{s,l}^H\mathbf{w}_i\right|^2+\left|\mathbf{h}_{s,l}^H\mathbf{P}\mathbf{v}\right|^2+\sigma^2\le e^{y_l},\quad\forall l,\tag{20c}$$

$$\sum_{j=1}^{L}\left|\mathbf{f}_{l,k}^H\mathbf{w}_j\right|^2+\left|\mathbf{h}_{l,k}^H\mathbf{P}\mathbf{v}\right|^2+\sigma^2\le e^{p_l},\quad\forall l,k,\tag{20d}$$

$$\sum_{i\neq l}^{L}\left|\mathbf{f}_{l,k}^H\mathbf{w}_i\right|^2+\left|\mathbf{h}_{l,k}^H\mathbf{P}\mathbf{v}\right|^2+\sigma^2\ge e^{q_l},\quad\forall l,k,\tag{20e}$$

$$(7b)-(7e).\tag{20f}$$

Authorized licensed use limited to: McGill University. Downloaded on November 21,2022 at 05:36:04 UTC from IEEE Xplore. Restrictions apply.

It is verified that the objective function (20a) is still nonconvex due to its fractional form. By introducing the positive auxiliary variables $\{t_2, \varsigma\}$, problem (20) can be transformed as

$$\begin{aligned}
&\max_{\substack{\mathbf{P},\mathbf{w}_l,\mathbf{v},t_2,\varsigma\\ x_l,y_l,p_l,q_l}} \quad t_2 \\
&\text{s.t.} \ \sum_{l=1}^{L} \mu_l \left(x_l - y_l - p_l + q_l\right) \geq t_2\varsigma, \\
&\qquad \eta_1 \sum_{l=1}^{L} \|\mathbf{w}_l\|^2 + \eta_2 \|\mathbf{v}\|^2 + P_S + P_B \leq \varsigma, \\
&\qquad (20b) - (20f).
\end{aligned} \tag{21}$$

Then, we introduce positive auxiliary variable d into the first constraint of (21), leading to

$$\begin{aligned}
&\sum_{l=1}^{L} \mu_l \left(x_l - y_l - p_l + q_l\right) \geq d^2 \\
&d^2 \geq t_2\varsigma
\end{aligned} \tag{22}$$

By using the first-order Taylor series expansion method to d and ζ, constraint (22) can be rewritten as the following LMI and SOC constraints

$$\begin{aligned}
&\frac{g+1}{2} \geq \left\| \left[\frac{g-1}{2}, d\right]^T \right\|_2, \\
&2\left(d^{(n)}/\zeta^{(n)}\right) d - \left(d^{(n)}/\zeta^{(n)}\right)^2 \zeta \geq t_2,
\end{aligned} \tag{23}$$

where $g = \sum_{l=1}^{L} \mu_l \left(x_l - y_l - p_l + q_l\right)$. Next, we focus on the constraints (20b)-(20e). To further reduce the computational complexity associated to the generalized nonlinear convex program of (20b), we approximate constrains (20b) and (20e) by a series of SOC forms described by

$$\begin{aligned}
&1 + z_{l,1} \geq \left\| \left[1 - z_{l,1}, 2 + x_l/2^{N-1}\right]^T \right\|_2, \\
&1 + z_{l,2} \geq \left\| \left[1 - z_{l,2}, 5/3 + x_l/2^{N}\right] \right\|_2, \\
&1 + z_{l,3} \geq \left\| \left[1 - z_{l,3}, 2z_{l,1}\right] \right\|_2, \\
&z_{l,4} \geq 19/72 + z_{l,2} + z_{l,3}/24, \\
&1 + z_{l,i} \geq \left\| \left[1 - z_{l,i}, 2z_{l,i-1}\right] \right\|_2, \ i = 5, \ldots, Q+3, \\
&1 + z_{l,Q+4} \geq \left\| \left[1 - z_{l,Q+4}, 2z_{l,Q+3}\right] \right\|_2,
\end{aligned} \tag{24a}$$

$$\sum_{j=1}^{L} \left|\mathbf{f}_{s,l}^H \mathbf{w}_j\right|^2 + \left|\mathbf{h}_{s,l}^H \mathbf{P}\mathbf{v}\right|^2 + \sigma^2 \geq 1 + z_{l,Q+4}. \tag{24b}$$

$$f_2\left(\mathbf{z}_{l,k}\right) \tag{25a}$$

$$\sum_{i\neq l}^{L} \left|\mathbf{f}_{l,k}^H \mathbf{w}_i\right|^2 + \left|\mathbf{h}_{l,k}^H \mathbf{P}\mathbf{v}\right|^2 + \sigma^2 \geq 1 + z_{l,k,Q+4}. \tag{25b}$$

where $\mathbf{z}_{l,k} = \left[z_{l,k,1}, \ldots, z_{l,k,Q+4}\right]^T, \forall l, k$ and $\mathbf{z}_l = \left[z_{l,1}, \ldots, z_{l,Q+4}\right]^T, \forall l$ are the introduced variables, the inequalities $f_2\left(\mathbf{z}_{l,k}\right)$ are similar to (24a) by replacing $\mathbf{z}_l$ with $\mathbf{z}_{l,k}$. The accuracy of (24) and (25) would increase as Q increases. We verify that the accuracy of (24) and (25) is on the order of 10^{-6} when $Q = 7$.

In addition, by applying the first-order Taylor series expansion to the right sides of (20c) and (20d) as $e^{y_l^{(n)}}(y_l - y_l^{(n)} + 1)$ and $e^{q_l^{(n)}}(q_l - q_l^{(n)} + 1)$, respectively, these two constraints at the n_1-th iteration can be approximated as

$$\begin{aligned}
&\sum_{i\neq l}^{L} \left|\mathbf{f}_{s,l}^H \mathbf{w}_i\right|^2 + \left|\mathbf{h}_{s,l}^H \mathbf{P}\mathbf{v}\right|^2 + \sigma^2 \leq e^{y_l^{(n)}}(y_l - y_l^{(n)} + 1), \\
&\sum_{j=1}^{L} \left|\mathbf{f}_{l,k}^H \mathbf{w}_j\right|^2 + \left|\mathbf{h}_{l,k}^H \mathbf{P}\mathbf{v}\right|^2 + \sigma^2 \leq e^{q_l^{(n)}}(q_l - q_l^{(n)} + 1).
\end{aligned} \tag{26}$$

The problem is still nonconvex due to the coupled variables $\mathbf{v}$ and $\mathbf{P}$. As in Section IV, we exploit the separate iterative optimization scheme and discretization method. After the n-th iteration, we obtain an analog precoder, $\mathbf{P}^{(n)}$, and the optimization problem on the digital beamformers can be expressed as

$$\max_{\substack{\mathbf{W}_l,\mathbf{V},t_2,d,\varsigma\\ x_l,y_l,p_l,q_l}} \quad t_2 \tag{27a}$$

$$\text{s.t.} \ \eta_1 \sum\nolimits_{l=1}^{L} \mathrm{Tr}\left(\mathbf{W}_l\right) + \eta_2 \mathrm{Tr}\left(\mathbf{V}\right) + P_S + P_B \leq \varsigma, \tag{27b}$$

$$\sum\nolimits_{j=1}^{L} \mathrm{Tr}\left(\mathbf{F}_{s,l}\mathbf{W}_j\right) + \mathrm{Tr}\left(\mathbf{P}^{(n)H}\mathbf{H}_{s,l}\mathbf{P}^{(n)}\bar{\mathbf{V}}\right) + \sigma^2 \geq 1 + z_{l,N+4}, \ \forall l, \tag{27c}$$

$$\sum\nolimits_{i\neq l}^{L} \mathrm{Tr}\left(\mathbf{F}_{s,l}\mathbf{W}_i\right) + \mathrm{Tr}\left(\mathbf{P}^{(n)H}\mathbf{H}_{s,l}\mathbf{P}^{(n)}\bar{\mathbf{V}}\right) + \sigma^2 \leq e^{y_l^{(n_1)}}(y_l - y_l^{(n_1)} + 1), \ \forall l, \tag{27d}$$

$$\sum\nolimits_{i\neq j}^{L} \mathrm{Tr}\left(\tilde{\mathbf{F}}_{l,k}\mathbf{W}_i\right) + \mathrm{Tr}\left(\mathbf{P}^{(n)H}\tilde{\mathbf{H}}_{l,k}\mathbf{P}^{(n)}\mathbf{V}\right) + \sigma^2 \geq 1 + z_{l,k,N+4}, \ \forall l, k \tag{27e}$$

$$\sum\nolimits_{j=1}^{L} \mathrm{Tr}\left(\tilde{\mathbf{F}}_{l,k}\mathbf{W}_j\right) + \mathrm{Tr}\left(\mathbf{P}^{(n)H}\tilde{\mathbf{H}}_{l,k}\mathbf{P}^{(n)}\mathbf{V}\right) + \sigma^2 \leq e^{p_l^{(n_1)}}(p_l - p_l^{(n_1)} + 1), \ \forall l, \tag{27f}$$

$$\mathrm{Tr}\left(\mathbf{P}^{(n)H}\mathbf{H}_{c,m}\mathbf{P}^{(n)}\mathbf{V}\right) - \Gamma_c\left(\sum\nolimits_{l=1}^{L} \mathrm{Tr}\left(\mathbf{F}_{c,m}\mathbf{W}_l\right) + \sigma^2\right) \geq 0, \ \forall m, \tag{27g}$$

$$\mathrm{Tr}\left(\mathbf{F}_{s,l}\mathbf{W}_l\right) - \Gamma_s\left(\sum\nolimits_{i\neq l}^{L} \mathrm{Tr}\left(\mathbf{F}_{s,l}\mathbf{W}_i\right) + \mathrm{Tr}\left(\mathbf{P}^{(n)H}\mathbf{H}_{s,l}\mathbf{P}^{(n)}\bar{\mathbf{V}}\right) + \sigma^2\right) \geq 0, \ \forall l, \tag{27h}$$

$$\mathrm{Tr}\left(\mathbf{V}\right) \leq P_b, \mathrm{Tr}\left(\mathbf{W}_l\right) \leq P_{s,l}, \ \forall l, \tag{27i}$$

$$\mathrm{rank}\left(\mathbf{V}\right) = 1, \mathrm{rank}\left(\mathbf{W}_l\right) = 1, \ \forall l, \tag{27j}$$

$$(23), (24a), (25a). \tag{27k}$$

It can be seen that the above iterative optimization problem is convex except for the rank-1 constraints (27j). To address this problem, by denoting $\mathbf{v}^{(n)}$ and $\mathbf{w}_l^{(n)}$ as the value of $\mathbf{v}$ and $\mathbf{w}_l$ at the n-th iteration, the matrix variables $\mathbf{V}$ and $\mathbf{W}_l$ can be approximated as

$$\begin{aligned}
\mathbf{V} &= \mathbf{v}^{(n)}\mathbf{v}^H + \mathbf{v}\mathbf{v}^{(n)H} - \mathbf{v}^{(n)}\mathbf{v}^{(n)H}, \\
\mathbf{W}_l &= \mathbf{w}_l^{(n)}\mathbf{w}_l^H + \mathbf{w}_l\mathbf{w}_l^{(n)H} - \mathbf{w}_l^{(n)}\mathbf{w}_l^{(n)H}.
\end{aligned} \tag{28}$$

Then, constraint (27j) can be removed since the iterative process will end only if $\mathbf{w}_l^{(n)} = \mathbf{w}_l^{(n-1)}$ and $\mathbf{v}^{(n)} = \mathbf{v}^{(n-1)}$, which guarantees that the rank of $\mathbf{W}_l$ and $\mathbf{V}$ is one.

Authorized licensed use limited to: McGill University. Downloaded on November 21,2022 at 05:36:04 UTC from IEEE Xplore. Restrictions apply.

Next, we focus on the analog precoder $\mathbf{P}$. Similar to the procedure for obtaining digital beamformers, after the n-th iteration, we have obtained digital beamformers $\mathbf{w}_l^{(n)}$ and $\mathbf{v}^{(n)}$, and the optimization problem (20) for the analog precoder can be expressed as

$$\max_{\hat{\mathbf{P}},x_l,y_l,p_l,q_l} \sum\nolimits_{l=1}^{L} \mu_l \left(x_l - y_l - p_l + p_l\right) \tag{29a}$$

$$\text{s.t.} \sum\nolimits_{j=1}^{L} \mathrm{Tr}\left(\mathbf{F}_{s,l}\mathbf{W}_j^{(n)}\right) + \mathrm{Tr}\left(\mathbf{V}^{(n)H}\tilde{\mathbf{H}}_{s,l}\mathbf{V}^{(n)}\hat{\mathbf{P}}\right) + \sigma^2 \geq 1 + z_{l,N+4}, \ \forall l, \tag{29b}$$

$$\sum\nolimits_{i\neq l}^{L} \mathrm{Tr}\left(\mathbf{F}_{s,l}\mathbf{W}_i^{(n)}\right) + \mathrm{Tr}\left(\mathbf{V}^{(n)H}\tilde{\mathbf{H}}_{s,l}\mathbf{V}^{(n)}\hat{\mathbf{P}}\right) + \sigma^2 \leq e^{y_l^{(n_1)}}(y_l - y_l^{(n_1)} + 1), \quad \forall l, \tag{29c}$$

$$\sum\nolimits_{i\neq j}^{L} \mathrm{Tr}\left(\tilde{\mathbf{F}}_{l,k}\mathbf{W}_i^{(n)}\right) + \mathrm{Tr}\left(\mathbf{V}^{(n)H}\tilde{\mathbf{H}}_{l,k}\mathbf{V}^{(n)}\hat{\mathbf{P}}\right) + \sigma^2 \geq 1 + z_{l,k,N+4}, \quad \forall l,k \tag{29d}$$

$$\sum\nolimits_{j=1}^{L} \mathrm{Tr}\left(\tilde{\mathbf{F}}_{l,k}\mathbf{W}_j^{(n)}\right) + \mathrm{Tr}\left(\mathbf{V}^{(n)H}\tilde{\mathbf{H}}_{l,k}\mathbf{V}^{(n)}\hat{\mathbf{P}}\right) + \sigma^2 \leq e^{p_l^{(n_1)}}(p_l - p_l^{(n_1)} + 1), \quad \forall l, \tag{29e}$$

$$\mathrm{Tr}\left(\mathbf{V}^{(n)H}\tilde{\mathbf{H}}_{c,m}\mathbf{V}^{(n)}\hat{\mathbf{P}}\right) - \Gamma_c\left(\sum\nolimits_{l=1}^{L} \mathrm{Tr}\left(\mathbf{F}_{c,m}\mathbf{W}_l^{(n)}\right) + \sigma^2\right) \geq 0, \quad \forall m, \tag{29f}$$

$$\mathrm{Tr}\left(\mathbf{F}_{s,l}\mathbf{W}_l^{(n)}\right) - \Gamma_s\left(\sum\nolimits_{i\neq l}^{L} \mathrm{Tr}\left(\mathbf{F}_{s,l}\mathbf{W}_i\right) + \mathrm{Tr}\left(\mathbf{V}^{(n)H}\tilde{\mathbf{H}}_{s,l}\mathbf{V}^{(n)}\hat{\mathbf{P}}\right) + \sigma^2\right) \geq 0, \quad \forall l, \tag{29g}$$

$$\mathrm{diag}[\hat{\mathbf{P}}]_q = \left[\mathbf{q}\mathbf{q}^H\right]_q, \quad q = 1, \cdots, N_b N_r, \tag{29h}$$

$$\mathrm{rank}(\hat{\mathbf{P}}) = 1, \tag{29i}$$

$$(30a). \tag{29j}$$

Different from optimization problem (27), the total power in objective (25a) and some constraints (namely (27b), (27i), (27j)) can be neglected because the digital beamformers are available at each iterative step when solving for $\hat{\mathbf{P}}$. Then, problem (29) can be efficiently solved through the nonsmooth method in Section IV, but the details are omitted for brevity. The proposed hybrid BF scheme for multiple ESs is summarized as Algorithm 2.

It is observed that problem (27) has been converted into a convex one by using (28), while the precondition for solving (27) is that the initial points $\mathbf{v}^{(0)}, \{\mathbf{w}_l^{(0)}, x_l^{(0)}, y_l^{(0)}, p_l^{(0)}, q_l^{(0)}\}$ are feasible to problem (29). In previous works, the initial points for this type of approach are randomly generated, which results in low convergence rate and sometimes infeasibility. Therefore, a low-complexity algorithm for calculating the initial points of problem (27) is important prior to using Algorithm 1 for optimizing the BF weight vectors. Due to space limitations, we only consider the digital beamformer optimization in (27); however, the same procedure can be employed for the analog beamformer optimization. We introduce a positive variable δ to measure how far the constraints of (29) are from being satisfied, and the initialization problem

Algorithm 2: The Proposed Hybrid BF Scheme With Multiple ESs

Input: $\{\mathbf{h}_{c,m}, \mathbf{h}_{l,k}, \mathbf{f}_{l,k}, \mathbf{f}_{s,l}, P_{s,l}\}$, Γ_c, Γ_s, and P_b.

1 Set the tolerance of accuracy ε_1 and ε_2;
2 Initialize the feasible precoder $\mathbf{P}^{(0)}$;
3 Set the iteration number $n_3 = 0$, $n_4 = 0$;
4 **repeat**
5 Initialize $\mathbf{w}_l^{(n_4)}, \mathbf{v}^{(n_4)}, y_l^{(n_4)}, p_l^{(n_4)}$, $\eta = 1$;
6 **while** $\eta \geq \varepsilon_2$ **do**
7 Set $n_4 := n_4 + 1$;
8 Solve the problem (27) with constraint (28);
9 Update $\mathbf{w}_l^{(n_4)}, \mathbf{v}^{(n_4)}, y_l^{(n_4)}, p_l^{(n_4)}$;
10 $\eta :=$ $\sum_{l=1}^{L}\left(\left\|\mathbf{w}_l^{(n_4)} - \mathbf{w}_l^{(n_4-1)}\right\|_F + \left|y_l^{(n_4)} - y_l^{(n_4-1)}\right| + \left|p_l^{(n_4)} - p_l^{(n_4-1)}\right|\right) + \left\|\mathbf{v}^{(n_4)} - \mathbf{v}^{(n_4-1)}\right\|_F$;
11 **end**
12 Obtain solutions $\mathbf{w}_l$ and $\mathbf{v}$, set $n_4 := 0, \mathbf{w}_l^{(n_3+1)} := \mathbf{w}_l, \mathbf{v}^{(n_3+1)} := \mathbf{v}$;
13 Initialize $y_l^{(n_4)}, p_l^{(n_4)}$, $\eta = 1$;
14 Compute $\mathbf{P}^{(n_3+1)}$ on problem (29) with similar procedure of *step* 6-11;
15 Set $n_3 := n_3 + 1$;
16 **until** $\left|\mathbf{P}^{(n_3)}\mathbf{v}^{(n_3)} - \mathbf{P}^{(n_3-1)}\mathbf{v}^{(n_3-1)}\right|^2 \leq \varepsilon_1$;

Output: Analog precoder $\mathbf{P}$, digital beamformers $\mathbf{w}_l$ and $\mathbf{v}$.

is formulated as

$$\max_{\substack{\delta,\mathbf{W}_l,\mathbf{V},d,\\ x_l,y_l,p_l,q_l}} \delta$$
$$\text{s.t. } (27b)^* - (27i)^*, (23)^*, (24a)^*, (25a)^* \text{ with } \mathbf{W}_l \text{ and } \mathbf{V} \text{ given by } (28) \tag{30}$$

where the constraint $(X)^* \in \{\text{constraints of } (X)\}$ corresponds to the modified version of (X) with δ. To obtain the constraints $(X)^*$, we first rewrite the constraint (X) as $f(x) \leq 0$, and then replace it with $f(x) \leq \delta$. Finally, the feasible initial points can be obtained by solving (27). The proposed algorithm for searching an initial point, summarized in Algorithm 3, is based on a similar iterative approximation method as the one adopted in Algorithm 2. Both Algorithms 2 and 3 are guaranteed to converge; the proof, which is omitted here for brevity, can be found in [16].

Remark 2: Note that when applying the proposed scheme in this Section to the single Eve scenario, the computational complexity is higher than that in Section III, while the SEE performance may be slightly worse. Hence, two hybrid BF design schemes are proposed respectively for the cases of single and multiple Eves.

V. Numerical Results

This section presents the results of numerical simulations to characterize the performance of the proposed hybrid BF schemes. We consider two scenarios with $L \in \{1, 2\}$ ESs, i.e. the satellite serves one and two ESs, respectively.

Authorized licensed use limited to: McGill University. Downloaded on November 21,2022 at 05:36:04 UTC from IEEE Xplore. Restrictions apply.

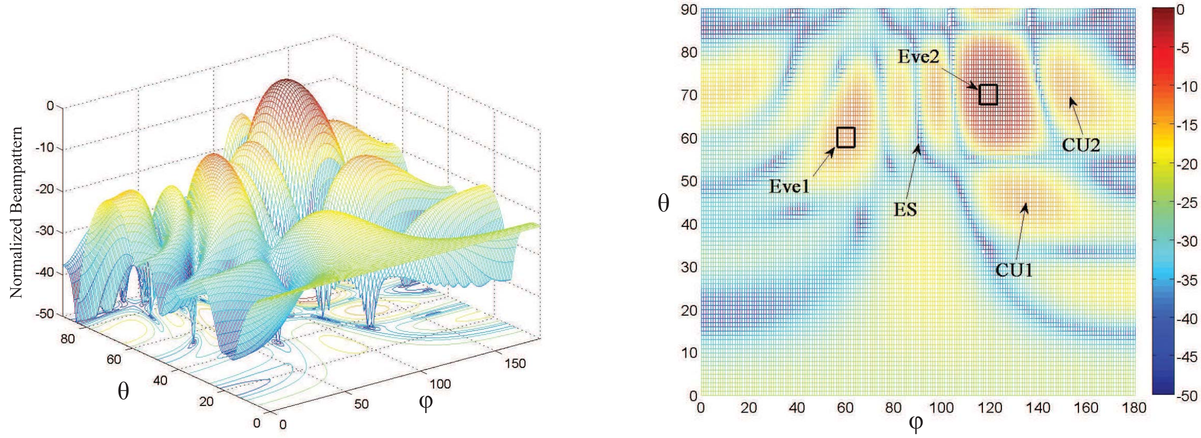

(a) Beampattern of $\mathbf{Pv}$

(b) Beampattern of $\mathbf{Pv}$ (top view)

Fig. 4. Beampattern of $\mathbf{Pv}$ with interleaved architecture.

Algorithm 3: Initial Point Search Algorithm

Input: $\{\mathbf{h}_{c,m}, \mathbf{h}_{l,k}, \mathbf{f}_{l,k}, \mathbf{f}_{s,l}, P_{s,l}\}$, Γ_c, Γ_s, and P_b.

Set the tolerance of accuracy ε_2 and the iteration number $n_5 = 0$;

Initialize the algorithm with random points $\mathbf{v}^{(0)}, \left\{\mathbf{w}_l^{(0)}, x_l^{(0)}, y_l^{(0)}, p_l^{(0)}, q_l^{(0)}\right\}$;

repeat

  $n_5 := n_5 + 1$;

  Solve the problem (35);

  Update $\mathbf{v}^{(n_5)}, \left\{\mathbf{w}_l^{(n_5)}, x_l^{(n_5)}, y_l^{(n_5)}, p_l^{(n_5)}, q_l^{(n_5)}\right\}$;

until $\delta < \varepsilon_2$;

Set $n_5 = 0$;

Output: $\mathbf{v}^{(0)}, \left\{\mathbf{w}_l^{(0)}, x_l^{(0)}, y_l^{(0)}, p_l^{(0)}, q_l^{(0)}\right\}$

TABLE II
MAIN SIMULATION PARAMETERS

Parameter	Value
Carrier frequency	18 GHz
Antenna inter-element spacing	$d_1 = d_2 = \lambda/2$
Number of satellite antennas	$N_s = 7$
Number of NLoS paths	$N = 5$
Maximal beam gain	$G_{\max} = 52$ dB
Bandwidth	B = 50 MHz
Off-boresight 3dB beamwidth	$\phi_{3\text{dB}} = 0.4°$
Noise temperature	T = 300 K
Rain fading	μ=-3.125, σ=1.591
3dB angle	$\theta_{3\text{dB}} = 10°$, $\varphi_{3\text{dB}} = 60°$

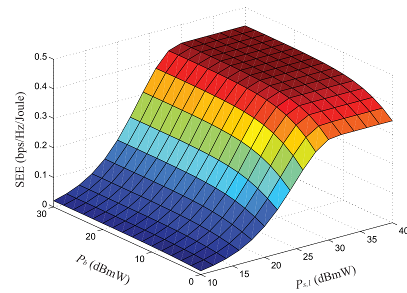

Fig. 5. SEE of interleaved architecture.

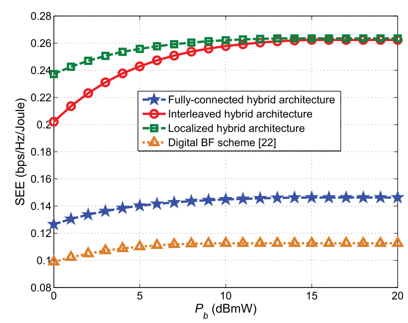

Fig. 6. SEE versus P_b.

Each ES is intercepted by $K_l = 2$ Eves, and the BS serves $M = 2$ CUs using broadcast communications. The SINR thresholds of the CUs and ESs are set as $\Gamma_c = \Gamma_s = -3$ dB, and the power amplifier inefficiency of satellite and BS as $\eta_1 = \eta_2 = 1/0.39$. The RF chains, the power amplifiers and the baseband processor power consumption of the satellite and BS are set as $P_{sr} = 400$ mW, $P_{br} = 250$ mW, $P_{sa} = 50$ mW, $P_{ba} = 20$ mW, $P_{sb} = P_{bb} = 300$ mW, respectively. The power consumption of the phase shifter, power splitter, and power combiner are set as $P_{bp} = 30$ mW, $P_{bs} = 10$ mW and $P_{bc} = 10$ mW [41]. The tolerance of accuracy is set as $\varepsilon_1 = \varepsilon_2 = 10^{-4}$, and the other parameters are listed in TABLE II. In the simulations, the digital BF scheme in [22] is adopted as a benchmark.

A. Single ES Scenario

We first consider the scenario of a single ES (Section III) and show the performance results in Figs. 4 to 9. Fig. 4(a) and Fig. 4(b) depict the beampattern of the combined BF

Authorized licensed use limited to: McGill University. Downloaded on November 21,2022 at 05:36:04 UTC from IEEE Xplore. Restrictions apply.

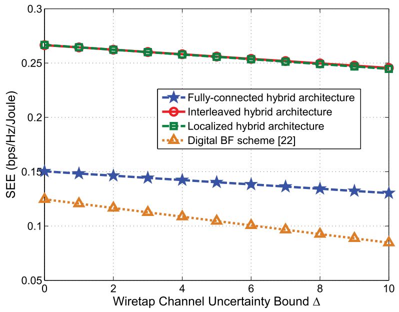

Fig. 7. SEE versus Δ.

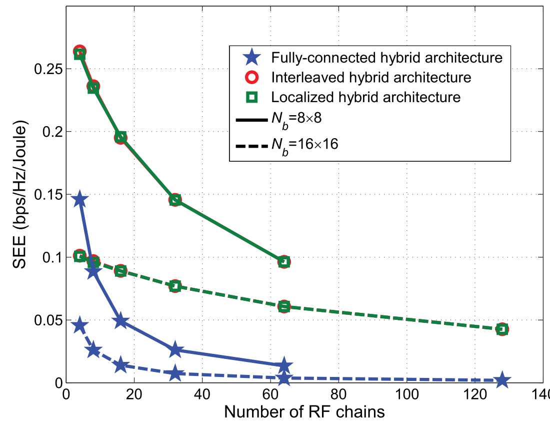

Fig. 8. SEE versus number of RF chains.

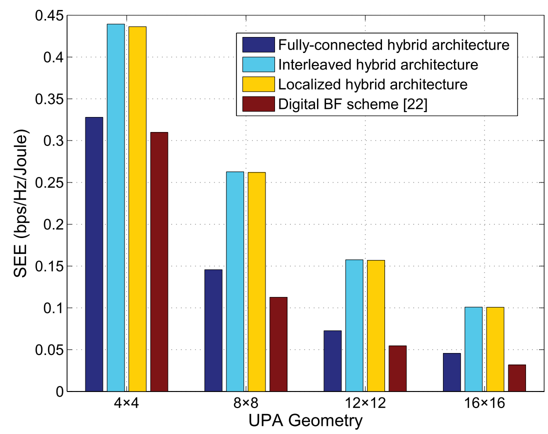

Fig. 9. SEE versus UPA geometry.

weight vector $\mathbf{Pv}$ of the proposed hybrid BF scheme with the interleaved architecture, where the transmit power budget of the SAT and BS are set as $P_b = P_{s,1} = 30$ dBmW, the channel uncertainty region $\Delta = 4°$, and the BS is equipped with a UPA comprising $N_b = 8 \times 8 = 64$ antennas. As we can see, the two main lobes of the beampattern point to the two Eves with a value of at least -10 dB in the uncertainty region of Eves. The received SINR of the intended CUs is also guaranteed at the required thresholds, while a null is generated with -45 dB at the ES. This figure demonstrates that the obtained BF weight vectors of the proposed hybrid BF scheme with interleaved architecture can efficiently generate interference towards Eves in the channel uncertainty region, improve the received signal quality at the intended users and simultaneously suppress the interference leakage at unintended users.

Fig. 5 plots the SEE of the interleaved hybrid array versus the transmit power budget of the satellite and BS, with $N_r = 4$ RF chains and a UPA of $N_b = 4 \times 4 = 16$ elements. It is clear that the SEE performance of the proposed scheme increases with increasing power budget of the satellite and BS, and gradually converges to a constant value. This is due to the fact that when the transmit power is large enough to achieve maximal SEE performance, further increasing the power budget will not lead to more power consumption to maintain the maximal SEE performance. It can also be observed that the effect of satellite power budget $P_{s,l}$ on SEE performance is greater than that of the BS power budget, which demonstrates that secure satellite downlink transmission can be easily guaranteed with limited interference power from the BS.

Figs. 6 and 7 depict the SEE versus the BS transmit power budget P_b and the wiretap channel uncertainty bound, respectively. We assume that the BS is equipped with a 8×8 UPA, and the other parameters are the same as those in Fig. 5. From Fig. 6, it is clear that our proposed BF scheme with three hybrid architectures always outperforms the digital scheme, and moreover the interleaved and localized architectures also achieve better performance than the fully-connected architecture. The reason is that the number of RF chains in the fully-digital architecture is much larger than that in the hybrid ones, thus causing additional power consumption and limited SEE performance. On the other hand, the fully-connected architecture contains $(N_r - 1)N_b$ more phase shifters than the other two sub-array architectures, leading to a performance gap compared with that in the interleaved and localized architectures. In Fig. 7, it can be seen that the proposed hybrid BF scheme achieves a more stable SEE performance than the digital BF scheme when the wiretap channel uncertainty bound becomes larger.

Figs. 8 and 9 depict the SEE versus the number of RF chains N_r and antennas at BS, respectively. From Fig. 8, one can observe that increasing N_r would decrease the SEE performance for each architecture. It is noted that increasing the number of RF chains can slightly improve the spectral efficiency, however, it also increases circuit power consumption and, in turn, degrades the SEE performance. We also observe that the SEE performance of the interleaved and localized architectures is more stable than that of the fully-connected architecture. This is expected because increasing N_r also increases the power consumption of the phase shifters. In Fig. 9, the SEE performances of the four array architectures decrease with the size of the UPA, while the three proposed schemes with hybrid architectures outperform the digital BF scheme. Furthermore, it is obtained that the achievable secrecy rate of the sub-array architecture with 8×8 UPA can reach to 2.1 bps/Hz while the energy efficiency of the BS can reach to 0.47 bps/Hz/Joule, which verify that our proposed schemes can achieve secure and efficient communications.

Authorized licensed use limited to: McGill University. Downloaded on November 21,2022 at 05:36:04 UTC from IEEE Xplore. Restrictions apply.

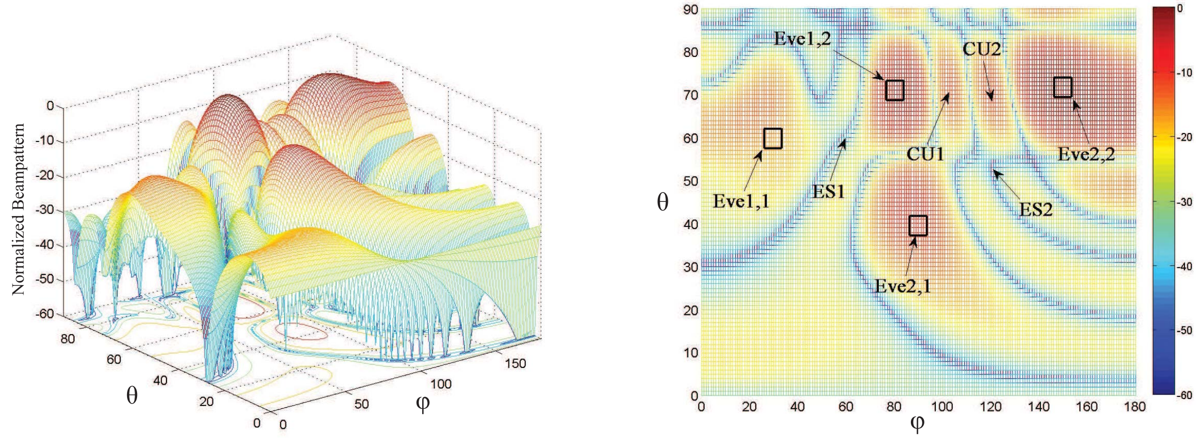

(a) Beampattern of $\mathbf{Pv}$ (b) Beampattern of $\mathbf{Pv}$ from vertical vision

Fig. 10. Beampattern of $\mathbf{Pv}$ with localized architecture.

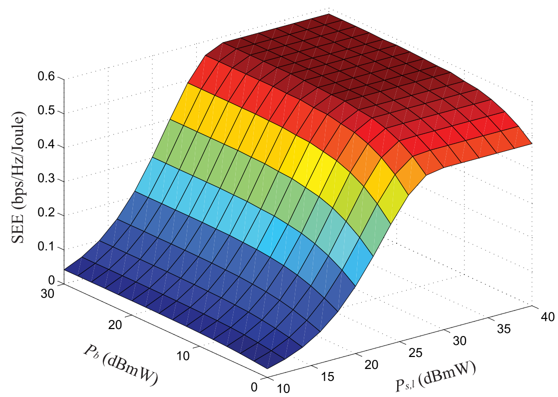

Fig. 11. SEE of localized sub-array with 4×4 antennas.

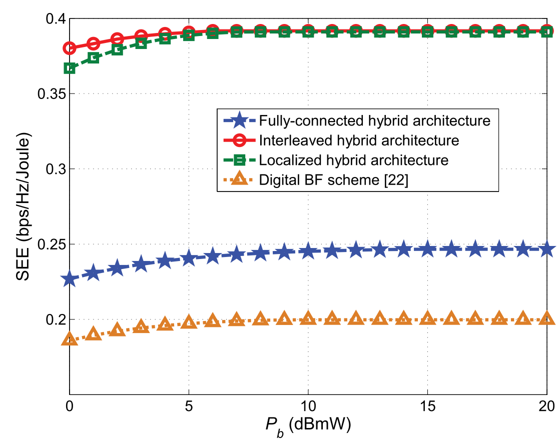

Fig. 12. SEE versus transmit power constraint of BS.

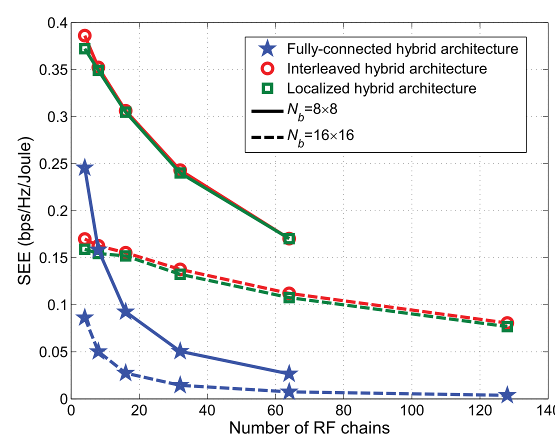

Fig. 13. SEE versus number of the RF chains.

B. Multiple ESs Scenario

Next, we consider the case of multiple ESs. Fig. 10(a) and Fig. 10(b) depict the beampattern of the combined BF weight vector $\mathbf{Pv}$ of the proposed scheme with the localized architecture, and the parameters are the same as those in Fig. 4. It can be observed that the four mainlobes of the beampattern point to the uncertainty region of the Eves with at least -10 dB interference, and the received SINRs of the intended CUs are guaranteed at required thresholds, while two nulls are generated with -40 dB at ESs.

Fig. 11 plots the SEE of the localized architecture versus the transmit power budget of the satellite and BS, with $N_r = 4$ RF chains and a $N_b = 4 \times 4 = 16$ UPA. We can observe that the SEE performance of the proposed scheme increases when increasing the power budget of the satellite and BS, and gradually converges to a constant value. Fig. 12 depicts the SEE versus the BS transmit power budget P_b with a $N_b = 8 \times 8 = 64$ UPA. It is clear that the proposed hybrid BF scheme with hybrid antenna architectures always outperforms the digital BF scheme, and moreover the hybrid BF scheme with interleaved and localized architectures also provide better performance than that with the fully-connected architecture. Comparing Figs. 11 and 12, we find that the SEE performance in Fig. 12 is only improved to a limited extent with increasing P_b. The reason is that the larger size of UPA in Fig. 12 provides a much higher antenna gain than the $N_b = 4 \times 4$ UPA in Fig. 11, and thus only limited BS power budget can generate intense interference signal towards the Eves and improve the SEE performance.

Furthermore, Figs. 13 and 14 present the SEE versus the number of RF chains N_r and the number of BS antennas N_b, respectively. From Fig. 13, we can observe that increasing N_r

Authorized licensed use limited to: McGill University. Downloaded on November 21,2022 at 05:36:04 UTC from IEEE Xplore. Restrictions apply.

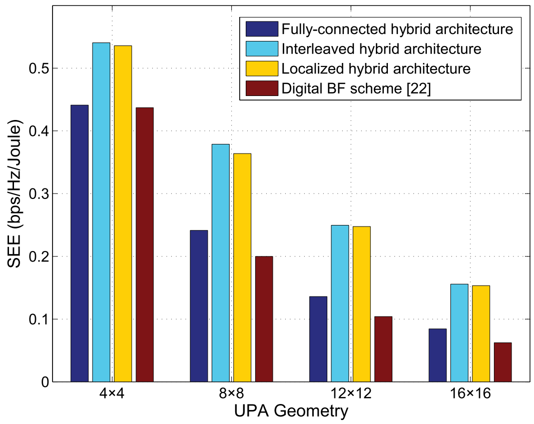

Fig. 14. SEE versus UPA geometry.

will decrease the SEE performance for each array architecture. In Fig. 14, the SEE performance of the proposed hybrid BF and digital BF schemes decreases with the size of the UPA, and the proposed schemes always outperform the digital BF scheme. Comparing the multiple ES case with the single ES one, the proposed hybrid BF scheme with interleaved architecture always outperforms that with the localized architecture for the multiple ESs case. The reason is that the array elements in each sub-array of the interleaved configuration are distributed in the whole array and the spacing between antenna elements in the sub-array is larger than that of the localized configuration, thus the beam pattern has narrower main and side lobes, which is more suitable for the multiuser scenario.

VI. Conclusion

In this paper, we presented a novel secrecy-energy efficient hybrid beamforming design for STIN operating in the mmWave band. By considering only the available imperfect knowledge of the AoDs for the wiretap channels, and employing hybrid array architectures, we solved the secrecy-energy efficiency maximization problem for single and multiple ES scenarios to meet the SINR constraints of both earth stations and cellular users. Specifically, we proposed two hybrid BF design schemes for the cases of single ES and multiple ESs, namely, the iterative BF scheme using Charnes-Cooper together with penalty function approaches, and the iterative BF scheme combined with the SCA approach. The advantage of the proposed hybrid BF schemes comes from the exploitation of interference from the BS to enhance the SEE performance for the ESs, and utilization of the hybrid analog-digital array for substantial reduction of the RF chains and power shifters' power consumption. Our simulation results demonstrated the superiority of the proposed hybrid BF schemes over the fully digital BF in the literature. We believe that our proposed BF scheme can provide an effective solution to enhance the SEE of the STIN.

Appendix

Proof of Proposition

Due to the discontinuous nature of the rank-1 constraint, it is difficult to directly solve problem (18) numerically. However, we can rewrite (14g) as

$$\begin{aligned} \mathrm{Tr}\left(\bar{\mathbf{W}}_1\right) - \lambda_{\max}\left(\bar{\mathbf{W}}_1\right) &\leq 0, \\ \mathrm{Tr}\left(\bar{\mathbf{V}}\right) - \lambda_{\max}\left(\bar{\mathbf{V}}\right) &\leq 0 \end{aligned} \tag{31}$$

where $\lambda_{\max}(\mathbf{X})$ denotes the maximal eigenvalue of matrix $\mathbf{X}$. Note that $\mathrm{Tr}(\mathbf{X}) \geq \lambda_{\max}(\mathbf{X})$ holds true for any positive semi-definite matrix. Hence, (31) implies that $\mathrm{Tr}(\mathbf{X}) = \lambda_{\max}(\mathbf{X})$ and $\mathbf{X}$ only has one positive eigenvalue, which can be expressed as

$$\begin{aligned} \bar{\mathbf{W}}_1 &= \lambda_{\max}\left(\bar{\mathbf{W}}_1\right)\bar{\mathbf{w}}_{1\max}\bar{\mathbf{w}}_{1\max}^H, \\ \bar{\mathbf{V}} &= \lambda_{\max}\left(\bar{\mathbf{V}}\right)\bar{\mathbf{v}}_{\max}\bar{\mathbf{v}}_{\max}^H \end{aligned} \tag{32}$$

where $\bar{\mathbf{w}}_{1\max}$ and $\bar{\mathbf{v}}_{\max}$ represent the corresponding eigenvectors of $\lambda_{\max}\left(\bar{\mathbf{W}}_1\right)$ and $\lambda_{\max}\left(\bar{\mathbf{V}}\right)$, respectively. Thus, problem (14) can be reformulated as

$$\begin{aligned} &\max_{\bar{\mathbf{W}}_1,\bar{\mathbf{V}},\beta} \ \beta\sigma^2 + \mathrm{Tr}\left(\mathbf{F}_{s,1}\bar{\mathbf{W}}_1\right) \\ &\quad \text{s.t.} \ (14b), (14d) - (14f), (15), (31). \end{aligned} \tag{33}$$

It should be mentioned that if $\mathrm{Tr}\left(\bar{\mathbf{W}}_1\right) - \lambda_{\max}\left(\bar{\mathbf{W}}_1\right)$ is small enough, $\mathrm{Tr}\left(\bar{\mathbf{W}}_1\right)$ can be approximated as $\lambda_{\max}\left(\bar{\mathbf{W}}_1\right)\bar{\mathbf{w}}_{1\max}\bar{\mathbf{w}}_{1\max}^H$. Thus, we aim at minimizing the difference of $\mathrm{Tr}\left(\bar{\mathbf{W}}_1\right) - \lambda_{\max}\left(\bar{\mathbf{W}}_1\right)$ (same for $\bar{\mathbf{V}}$). By using the penalty function method to substitute the constraint (31) into the objective function in (33), we obtain

$$\begin{aligned} &\max_{\bar{\mathbf{W}}_1,\bar{\mathbf{V}},\beta} \ \beta\sigma^2 + \mathrm{Tr}\left(\mathbf{F}_{s,1}\bar{\mathbf{W}}_1\right) - \mu_1\left(\mathrm{Tr}\left(\bar{\mathbf{W}}_1\right) - \lambda_{\max}\left(\bar{\mathbf{W}}_1\right)\right) \\ &\qquad - \mu_v\left(\mathrm{Tr}\left(\bar{\mathbf{V}}\right) - \lambda_{\max}\left(\bar{\mathbf{V}}\right)\right) \\ &\quad \text{s.t.} \ (14b), (14d) - (14f), (15). \end{aligned} \tag{34}$$

where μ_1 and μ_v are weighting coefficients, which are large enough to enforce the minimization of $\mathrm{Tr}\left(\bar{\mathbf{W}}_1\right) - \lambda_{\max}\left(\bar{\mathbf{W}}_1\right)$ and $\mathrm{Tr}\left(\bar{\mathbf{V}}\right) - \lambda_{\max}\left(\bar{\mathbf{V}}\right)$. It can be observed that (34) belongs to the class of concave programming due to the nonsmooth nature of $\lambda_{\max}\left(\bar{\mathbf{W}}_1\right)$ and $\lambda_{\max}\left(\bar{\mathbf{V}}\right)$. By using the subgradient version of the maximal eigenvalue function $\frac{\partial\lambda_{\max}(\mathbf{X})}{\partial\mathbf{x}} = \mathbf{x}_{\max}\mathbf{x}_{\max}^H$, we have

$$\begin{aligned} \lambda_{\max}(\mathbf{X}) - \lambda_{\max}\left(\bar{\mathbf{W}}_1\right) &= \left\langle \bar{\mathbf{w}}_{1\max}\bar{\mathbf{w}}_{1\max}^H, \mathbf{X} - \bar{\mathbf{W}}_1 \right\rangle, \\ \lambda_{\max}(\mathbf{X}) - \lambda_{\max}\left(\bar{\mathbf{V}}\right) &= \left\langle \bar{\mathbf{v}}_{\max}\bar{\mathbf{v}}_{\max}^H, \mathbf{X} - \bar{\mathbf{V}} \right\rangle. \end{aligned} \tag{35}$$

Then, by initializing the feasible matrices $\bar{\mathbf{W}}_1^{(n)}$ and $\bar{\mathbf{V}}^{(n)}$, and the corresponding eigenvectors $\bar{\mathbf{w}}_{1\max}^{(n)}$ and $\bar{\mathbf{v}}_{\max}^{(n)}$ of the maximal eigenvalues, problem (34) can be expressed as

$$\begin{aligned} &\max_{\bar{\mathbf{W}}_1,\bar{\mathbf{V}},\beta} \ \beta\sigma^2 + \mathrm{Tr}\left(\mathbf{F}_{s,1}\bar{\mathbf{W}}_1\right) \\ &\qquad - \mu_1\left(\mathrm{Tr}\left(\bar{\mathbf{W}}_1\right) - \left\langle \bar{\mathbf{w}}_{1\max}^{(n)}\bar{\mathbf{w}}_{1\max}^{(n)H}, \bar{\mathbf{W}}_1 \right\rangle\right) \\ &\qquad - \mu_v\left(\mathrm{Tr}\left(\bar{\mathbf{V}}\right) - \left\langle \bar{\mathbf{v}}_{\max}^{(n)}\bar{\mathbf{v}}_{\max}^{(n)H}, \bar{\mathbf{V}} \right\rangle\right) \\ &\quad \text{s.t.} \ (14b), (14d) - (14f), (15). \end{aligned} \tag{36}$$

which completes the proof.

It can be verified that the iterative problem (36) is convergent [15].

Authorized licensed use limited to: McGill University. Downloaded on November 21,2022 at 05:36:04 UTC from IEEE Xplore. Restrictions apply.

References

[1] M. Agiwal, A. Roy, and N. Saxena, "Next generation 5G wireless networks: A comprehensive survey," *IEEE Commun. Surveys Tuts.*, vol. 18, no. 3, pp. 1617–1655, 3rd Quart., 2016.

[2] K. An and T. Liang, "Hybrid satellite-terrestrial relay networks with adaptive transmission," *IEEE Trans. Veh. Technol.*, vol. 68, no. 12, pp. 12448–12452, Dec. 2019.

[3] M. A. Vazquez *et al.*, "Precoding in multibeam satellite communications: Present and future challenges," *IEEE Wireless Commun.*, vol. 23, no. 6, pp. 88–95, Dec. 2016.

[4] Y. Ruan, Y. Li, C.-X. Wang, R. Zhang, and H. Zhang, "Energy efficient power allocation for delay constrained cognitive satellite terrestrial networks under interference constraints," *IEEE Trans. Wireless Commun.*, vol. 18, no. 10, pp. 4957–4969, Oct. 2019.

[5] Z. Lin, M. Lin, T. de Cola, J.-B. Wang, W.-P. Zhu, and J. Cheng, "Supporting IoT with rate-splitting multiple access in satellite and aerial integrated networks," *IEEE Internet Things J.*, early access, Jan. 14, 2021, doi: 10.1109/JIOT.2021.3051603.

[6] K. An, Y. Li, T. Liang, and X. Yan, "On the performance of cache-enabled hybrid satellite-terrestrial relay networks," *IEEE Wireless Commun. Lett.*, vol. 8, no. 5, pp. 1506–1509, Jun. 2019.

[7] J. Du, C. Jiang, H. Zhang, X. Wang, Y. Ren, and M. Debbah, "Secure satellite-terrestrial transmission over incumbent terrestrial networks via cooperative beamforming," *IEEE J. Sel. Areas Commun.*, vol. 36, no. 7, pp. 1367–1382, Jul. 2018.

[8] Z. Lin, M. Lin, B. Champagne, W.-P. Zhu, and N. Al-Dhahir, "Secure and energy efficient transmission for RSMA-based cognitive satellite-terrestrial networks," *IEEE Wireless Commun. Lett.*, vol. 10, no. 2, pp. 251–255, Feb. 2021.

[9] Z. Lin, M. Lin, B. Champagne, W.-P. Zhu, and N. Al-Dhahir, "Secure beamforming for cognitive satellite terrestrial networks with unknown eavesdroppers," *IEEE Syst. J.*, vol. 15, no. 2, pp. 2186–2189, Jun. 2021.

[10] Z. Lin, M. Lin, J. Ouyang, W.-P. Zhu, and S. Chatzinotas, "Beamforming for secure wireless information and power transfer in terrestrial networks coexisting with satellite networks," *IEEE Signal Process. Lett.*, vol. 25, no. 8, pp. 1166–1170, Aug. 2018.

[11] S. K. Sharma, S. Chatzinotas, and B. Ottersten, "Transmit beamforming for spectral coexistence of satellite and terrestrial networks," in *Proc. 8th Int. Conf. Cognit. Radio Oriented Wireless Netw.*, Jul. 2013, pp. 275–281.

[12] F. Zhou, Z. Chu, H. Sun, R. Q. Hu, and L. Hanzo, "Artificial noise aided secure cognitive beamforming for cooperative MISO-NOMA using SWIPT," *IEEE J. Sel. Areas Commun.*, vol. 36, no. 4, pp. 918–931, Apr. 2018.

[13] G. Zheng, P.-D. Arapoglou, and B. Ottersten, "Physical layer security in multibeam satellite systems," *IEEE Trans. Wireless Commun.*, vol. 11, no. 2, pp. 852–863, Feb. 2012.

[14] K. An, M. Lin, J. Ouyang, and W.-P. Zhu, "Secure transmission in cognitive satellite terrestrial networks," *IEEE J. Sel. Areas Commun.*, vol. 34, no. 11, pp. 3025–3037, Nov. 2016.

[15] Z. Lin, M. Lin, W.-P. Zhu, J.-B. Wang, and J. Cheng, "Robust secure beamforming for wireless powered cognitive satellite-terrestrial networks," *IEEE Trans. Cognit. Commun. Netw.*, vol. 7, no. 2, pp. 567–580, Jun. 2021.

[16] Z. Lin, M. Lin, J.-B. Wang, T. de Cola, and J. Wang, "Joint beamforming and power allocation for satellite-terrestrial integrated networks with non-orthogonal multiple access," *IEEE J. Sel. Topics Signal Process.*, vol. 13, no. 3, pp. 657–670, Jun. 2019.

[17] Q. Huang, M. Lin, J.-B. Wang, T. A. Tsiftsis, and J. Wang, "Energy efficient beamforming schemes for satellite-aerial-terrestrial networks," *IEEE Trans. Commun.*, vol. 68, no. 6, pp. 3863–3875, Jun. 2020.

[18] Y. Lu, K. Xiong, P. Fan, Z. Ding, Z. Zhong, and K. B. Letaief, "Global energy efficiency in secure MISO SWIPT systems with non-linear power-splitting EH model," *IEEE J. Sel. Areas Commun.*, vol. 37, no. 1, pp. 216–232, Jan. 2019.

[19] L. Sboui, Z. Rezki, A. Sultan, and M.-S. Alouini, "A new relation between energy efficiency and spectral efficiency in wireless communications systems," *IEEE Wireless Commun.*, vol. 26, no. 3, pp. 168–174, Jun. 2019.

[20] P. Chen, J. Ouyang, W.-P. Zhu, and M. Lin, "Energy efficient beamforming for multi-user transmission in cognitive radio networks with secrecy constraints," *IEEE Access*, vol. 6, pp. 74485–74493, 2018.

[21] J. Ouyang, M. Lin, Y. Zou, W.-P. Zhu, and D. Massicotte, "Secrecy energy efficiency maximization in cognitive radio networks," *IEEE Access*, vol. 5, pp. 2641–2650, 2017.

[22] Y. Jiang, Y. Zou, J. Ouyang, and J. Zhu, "Secrecy energy efficiency optimization for artificial noise aided physical-layer security in OFDM-based cognitive radio networks," *IEEE Trans. Veh. Technol.*, vol. 67, no. 12, pp. 11858–11872, Dec. 2018.

[23] L. Ni, X. Da, H. Hu, Y. Yuan, Z. Zhu, and Y. Pan, "Outage-constrained secrecy energy efficiency optimization for CRNs with non-linear energy harvesting," *IEEE Access*, vol. 7, pp. 175213–175221, 2019.

[24] M. K. Arti, "Imperfect CSI based multi-way satellite relaying," *IEEE Wire. Commun. Lett.*, vol. 7, no. 1, pp. 62–65, Jan. 2018.

[25] M. K. Arti, "Channel estimation and detection in hybrid satellite–terrestrial communication systems," *IEEE Trans. Veh. Technol.*, vol. 65, no. 7, pp. 5764–5771, Jul. 2016.

[26] J. Huang and A. L. Swindlehurst, "Robust secure transmission in MISO channels based on worst-case optimization," *IEEE Trans. Signal Process.*, vol. 60, no. 4, pp. 1696–1707, Apr. 2012.

[27] S. Ma, Y. He, H. Li, S. Lu, F. Zhang, and S. Li, "Optimal power allocation for mobile users in non-orthogonal multiple access visible light communication networks," *IEEE Trans. Commun.*, vol. 67, no. 3, pp. 2233–2244, Mar. 2019.

[28] B. Li, Z. Fei, X. Xu, and Z. Chu, "Resource allocations for secure cognitive satellite-terrestrial networks," *IEEE Wireless Commun. Lett.*, vol. 7, no. 1, pp. 78–81, Feb. 2018.

[29] S. Ma, M. Hong, E. Song, X. Wang, and D. Sun, "Outage constrained robust secure transmission for MISO wiretap channels," *IEEE Trans. Wireless Commun.*, vol. 13, no. 10, pp. 5558–5570, Oct. 2014.

[30] B. Li, Z. Fei, Z. Chu, F. Zhou, K.-K. Wong, and P. Xiao, "Robust chance-constrained secure transmission for cognitive satellite–terrestrial networks," *IEEE Trans. Veh. Technol.*, vol. 67, no. 5, pp. 4208–4219, May 2018.

[31] W. Shi and J. Ritcey, "Robust beamforming for MISO wiretap channel by optimizing the worst-case secrecy capacity," in *Proc. Conf. Rec. Forty 4th Asilomar Conf. Signals, Syst. Comput.*, Nov. 2010, pp. 300–304.

[32] Z. Lin, M. Lin, B. Champagne, W.-P. Zhu, and N. Al-Dhahir, "Robust hybrid beamforming for satellite-terrestrial integrated networks," in *Proc. IEEE Int. Conf. Acoust., Speech Signal Process. (ICASSP)*, May 2020, pp. 1–5.

[33] Z. Lin, M. Lin, J.-B. Wang, Y. Huang, and W.-P. Zhu, "Robust secure beamforming for 5G cellular networks coexisting with satellite networks," *IEEE J. Sel. Areas Commun.*, vol. 36, no. 4, pp. 932–945, Apr. 2018.

[34] A. F. Molisch *et al.*, "Hybrid beamforming for massive MIMO: A survey," *IEEE Commun. Mag.*, vol. 55, no. 9, pp. 134–141, Sep. 2017.

[35] I. Ahmed *et al.*, "A survey on hybrid beamforming techniques in 5G: Architecture and system model perspectives," *IEEE Commun. Surveys Tuts.*, vol. 20, no. 4, pp. 3060–3097, 4th Quart. 2018.

[36] M. A. Vazquez, L. Blanco, X. Artiga, and A. Perez-Neira, "Hybrid analog-digital transmit beamforming for spectrum sharing satellite-terrestrial systems," in *Proc. IEEE 17th Int. Workshop Signal Process. Adv. Wireless Commun. (SPAWC)*, Jul. 2016, pp. 1–5.

[37] W. Dinkelbach, "On nonlinear fractional programming," *Manage. Sci.*, vol. 13, no. 7, pp. 492–498, Mar. 1967. [Online]. Available: http://www.jstor.org/stable/2627691

[38] Z. Lin, M. Lin, J. Ouyang, W.-P. Zhu, A. D. Panagopoulos, and M.-S. Alouini, "Robust secure beamforming for multibeam satellite communication systems," *IEEE Trans. Veh. Technol.*, vol. 68, no. 6, pp. 6202–6206, Jun. 2019.

[39] S. He, C. Qi, Y. Wu, and Y. Huang, "Energy-efficient transceiver design for hybrid sub-array architecture MIMO systems," *IEEE Access*, vol. 4, pp. 9895–9905, 2016.

[40] F. Shu *et al.*, "Low-complexity and high-resolution DOA estimation for hybrid analog and digital massive MIMO receive array," *IEEE Trans. Commun.*, vol. 66, no. 6, pp. 2487–2501, Jun. 2018.

[41] X. Gao, L. Dai, and A. M. Sayeed, "Low RF-complexity technologies to enable millimeter-wave MIMO with large antenna array for 5G wireless communications," *IEEE Commun. Mag.*, vol. 56, no. 4, pp. 211–217, Apr. 2018.

Authorized licensed use limited to: McGill University. Downloaded on November 21,2022 at 05:36:04 UTC from IEEE Xplore. Restrictions apply.

Zhi Lin received the B.E. and M.E. degrees in information and communication engineering from the PLA University of Science and Technology and the Ph.D. degree in electronic science and technology from the Army Engineering University of PLA, Nanjing, China, in 2013, 2016, and 2020, respectively. From March 2019 to June 2020, he was a visiting student with the Department of Electrical and Computer Engineering, McGill University, Canada. He is currently working with the Institute of Electronic Countermeasure, National University of Defense Technology, Hefei, China. His research interests include wireless communications, convex optimization, and array signal processing. He was a TPC member of many IEEE sponsored conferences, including IEEE ICC, Globecom, Infocom, VTC, and so on.

Min Lin (Member, IEEE) received the B.S. degree from the National University of Defense Technology, Changsha, China, in 1993, the M.S. degree from the Nanjing Institute of Communication Engineering, Nanjing, China, in 2000, and the Ph.D. degree from Southeast University, Nanjing, in 2008, all in electrical engineering. From April 2015 to October 2015, he has visited the University of California at Irvine, as a Senior Research Fellow. He is currently a Professor and a Supervisor of Ph.D. and graduate students with the Nanjing University of Posts and Telecommunications, Nanjing. He has authored or coauthored over 130 articles. His current research interests include wireless communications and array signal processing. He has served for the Track Chair of Satellite and Space Communications (SSC) of IEEE ICC 2019 and IEEE GLOBECOM 2021, and a TPC member of many IEEE sponsored conferences.

Benoit Champagne (Senior Member, IEEE) received the B.Ing. degree in engineering physics from École Polytechnique de Montréal, in 1983, the M.Sc. degree in physics from Université de Montréal, in 1985, and the Ph.D. degree in electrical engineering from the University of Toronto, in 1990. From 1990 to 1999, he was an Assistant and then an Associate Professor at INRS-Telecommunications, Universit du Quebec, Montreal. In 1999, he joined with McGill University, Montreal, where he is currently a Professor with the Department of Electrical and Computer Engineering. He served for an Associate Chairman of Graduate Studies with the Department, from 2004 to 2007. He has coauthored more than 300 referred publications. His research focuses on the study of advanced methods and algorithms for the processing of information bearing signals by digital means. His interests span many areas of statistical signal processing and machine learning, including detection and estimation, sensor array processing, adaptive filtering, and applications thereof to broadband communications, and audio processing. His research has been through the Natural Sciences and Engineering Research Council (NSERC), Canada, the Fonds de Recherche sur la Nature et les Technologies, Government of Quebec, as well as some major industrial sponsors, including Nortel Networks, Bell Canada, InterDigital, and Microchip. He has been an Associate Editor for the IEEE Signal Processing Letters, IEEE TRANSACTION ON SIGNAL PROCESSING, and the *EURASIP Journal on Applied Signal Processing*. He has also served for the Technical Committees of several international conferences in the fields of communications and signal processing.

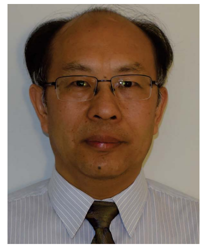

Wei-Ping Zhu (Senior Member, IEEE) received the B.E. and M.E. degrees from the Nanjing University of Posts and Telecommunications, Nanjing, China, and the Ph.D. degree from Southeast University, Nanjing, in 1982, 1985, and 1991, respectively, all in electrical engineering.

He was a Postdoctoral Fellow, from 1991 to 1992 and a Research Associate with the Department of Electrical and Computer Engineering, Concordia University, Montreal, Canada, from 1996 to 1998. From 1993 to 1996, he was an Associate Professor with the Department of Information Engineering, Nanjing University of Posts and Telecommunications. From 1998 to 2001, he worked with hi-tech companies, Ottawa, Canada, including Nortel Networks and SR Telecom Inc. Since July 2001, he has been with the Concordia's Electrical and Computer Engineering Department as a full-time Faculty Member, where he is presently a Full Professor. Since 2008, he has been an Adjunct Professor with the Nanjing University of Posts and Telecommunications. His research interests include digital signal processing fundamentals, speech and statistical signal processing, and signal processing for wireless communication with a particular focus on MIMO systems, and cooperative communication.

Dr. Zhu served as an Associate Editor for IEEE TRANSACTIONS ON CIRCUITS AND SYSTEMS, from 2001 to 2003 and from 2011 to 2015, respectively, and an Associate Editor for Circuits, Systems and Signal Processing, from 2006 to 2009. He was also a Guest Editor for IEEE JOURNAL ON SELECTED AREAS IN COMMUNICATIONS for the special issues of: Broadband Wireless Communications for High Speed Vehicles and Virtual MIMO, from 2011 to 2013. He is currently an Associate Editor of *Journal of The Franklin Institute*. He was the Secretary of Digital Signal Processing Technical Committee (DSPTC) of the IEEE Circuits and System Society, from June 2012 to May 2014, and the Chair of the DSPTC, from June 2014 to May 2016.

Naofal Al-Dhahir (Fellow, IEEE) received the Ph.D. degree from Stanford University. He is an Erik Jonsson Distinguished Professor with the ECE Department and an Associate Head at UT-Dallas. He was the Principal Member of Technical Staff at the AT and T Shannon Laboratory, GE Research Center, from 1994 to 2003. He is a co-inventor of 43 issued patents, coauthor of about 470 articles and co-recipient of four IEEE Best Paper Awards, and an IEEE SPCC Technical Recognition Award in 2021 and Qualcomm Faculty Award.

He served as an Editor-in-Chief for IEEE TRANSACTIONS ON COMMUNICATIONS, from January 2016 to December 2019. He is a fellow of the National Academy of Inventors.

Authorized licensed use limited to: McGill University. Downloaded on November 21,2022 at 05:36:04 UTC from IEEE Xplore. Restrictions apply.